Yarkovsky footprints in the Eos family

D. Vokrouhlický and M. Brož
Institute of Astronomy, Charles University, V Holešovičkách 2, 18000 Prague 8, Czech Republic

A. Morbidelli
Observatoire de la Côte d'Azur, BP 4229, 06304 Nice Cedex 4, France

W.F. Bottke and D. Nesvorný
Southwest Research Institute, 1050 Walnut St, Suite 400, Boulder, CO 80302, USA

D. Lazzaro
Observatorio Nacional, Rua Gal. Jose Cristino 77, 20921-400 Rio de Janeiro, Brazil

A.S. Rivkin[1]
Massachusetts Institute of Technology, 77 Massachusetts Av., Cambridge, MA 02139, USA

ABSTRACT

The Eos asteroid family is the third most populous, after Themis and Koronis, and one of the largest non-random groups of asteroids in the main belt. It has been known and studied for decades, but its structure and history still presented difficulties to understand. We first revise the Eos family identification as a statistical cluster in the space of proper elements. Using the most to-date catalogue of proper elements we determine a nominal Eos family, defined by us using the hierarchical-clustering method with the cut-off velocity of 55 m/s, contains some 4400 members. This unforeseen increase in known Eos asteroids allows us to perform a much more detailed study than was possible so far. We show, in particular, that most of the previously thought peculiar features are explained within the following model: (i) collisional disruption of the parent body leads to formation of a compact family in the proper element space (with characteristic escape velocities of the observed asteroids of tens of metres per second, compatible with hydrocode simulations), and (ii) as time goes, the family dynamically evolves due to a combination of the thermal effects and planetary perturbations. This model allows us to explain sharp termination of the family at the 7/3 mean motion resonance with Jupiter, uneven distribution of family members about the 9/4 mean motion resonance with Jupiter, semimajor axis distribution of large vs. small members in the family and anomalous residence of Eos members inside the high-order secular resonance z_1. Our dynamical method also allows us to estimate Eos family age to $1.3^{+0.15}_{-0.2}$ Gy. Several formal members of the Eos family are in conflict with our model and these are suspected interlopers. We use spectroscopic observations, whose results are also reported here, and results of 5-color wide-band Sloan Digital Sky Survey photometry to prove some of them are indeed spectrally incompatible with the family.

Subject headings: asteroids, asteroid families, Yarkovsky effect

1. Introduction and history in brief

Analysis of asteroid families has been a flourishing subject over past years mainly because of a discovery of previously unknown, very compact clusters of small asteroids (e.g. Nesvorný et al., 2002b, 2003; Nesvorný and Bottke, 2004). This possibility has been allowed by an unprecedented increase of known asteroids over the past decade which is mainly due to automated search programs for objects residing on planet crossing orbits (e.g. Stokes et al., 2002). The break-through achievement was an accurate determination of ages of these new young families via direct orbital integration. This has opened a wide range of implications in planetary science, such as a study of binary pairs and rotation properties among ejecta from collisional disruptions (REF???), fresh surfaces unaltered by space weathering processes (Jedicke et al., 2004; Nesvorný et al., 2005a) or origin of the IRAS/COBE dust bands (e.g. Nesvorný et al., 2002b, 2003, 2005b).

Here, however, we focus our analysis on the Eos family, one of the largest and long-studied structures in the main asteroid belt; the classical early references are Hirayama (1918) and Brouwer (1951), with more work done from the 1970s on (see the overview by Bendjoya and Zappalà, 2002). The seminal work of Brouwer (1951) is of interest for us, because it was first shown here that in spite of its high compactness, thus undisputable evidence, the Eos family presents some puzzling features that cannot be easily reconciled with a standard model. Brouwer noticed a tight width of the Eos family in semimajor axis (see Table IV in his paper), anomalously small as compared to its extension in proper eccentricity and proper inclination. Rightly defending the collisional model for the origin of the asteroid families, Brouwer got puzzled by a distorted velocity field corresponding to the observed distribution of the family in the proper element space.[2] To circumvent the problem he assumed inadequacies of the linear secular theory more likely affect eccentricity and inclination with errors, but he seemed to feel uncomfortable with this explanation.

A second issue raised by Brouwer (1951) were speculations about the age of this family that lasted for several decades. This is also very interesting for us, because the family age determines the timescale of its possible dynamical evolution. Chronology of asteroid families as accurate as possible is also a vital clue for understanding collisional evolution of the main asteroid belt (e.g. Bottke et al., 2005a,b). Brouwer noticed that within the simplest, linearized secular theory the sum of proper longitude of pericenter ϖ_p and proper longitude of node Ω_p holds constant because their related proper frequencies are exactly opposite. He thus proposed to use $(\varpi_p+\Omega_p)$ as an additional parameter to test properties of asteroid families. In particular, any strong clustering in this parameter should suggest a very young age of the family (presumably less than $\simeq 1$ My), because more accurate secular theory is expected to inevitably break this property. Brouwer (1951; see Table V) suggested the distribution of $(\varpi_p + \Omega_p)$ for Eos members known to him is strongly non-uniform, perhaps supporting the hypothesis of this family's young age. In spite of Carpino et al.'s (1986) finding that the $(\varpi_p + \Omega_p)$ time variation is anomalously slow in this particular zone of the main asteroid belt, Farinella et al. (1989) critically reassessed Brouwer's argument concluding it might have been fluke due to a small number of known members. By associating smaller asteroids with the family, these authors proved $(\varpi_p + \Omega_p)$ is quite more uniform, while residual non-uniformity suggesting perhaps only a younger subcluster of a limited number of members inside the Eos family. Arguing on base of the low probability for the Eos parent body disruption, Farinella et al. (1989) leaned toward a large age of the family (supported also by models of rotation period distribution for the family members; Binzel, 1988), dismissing thus usefulness of the $(\varpi_p + \Omega_p)$ parameter for family studies.[3] This is also our point of view; in Sec. 3.3 we check that this parame-

[1] Visiting Astronomer, Kitt Peak National Observatory, National Optical Astronomy Observatory, which is operated by the Association of Universities for Research in Astronomy, Inc. (AURA) under cooperative agreement with the National Science Foundation.

[2] For a historical curiosity, we mention that Brouwer (1951) was actually opposing to skepticism of Brown (1932) who believed that analysis of the origin of asteroid families is condemned to failure for effects of many unknown perturbations, including *those of non-gravitational origin* (cit.).

[3] The only exception is the case of very young families; Nesvorný et al. (2002b, 2003).

ter obeys a near uniform distribution with deviations compatible with statistical fluctuations and the expected influence of the secular resonance z_1 (compare with Milani and Knežević, 1992, 1994).

The problem of Eos age has been reiterated by Morbidelli et al. (1995) who studied asteroid families close (or intercepted by) mean motion resonances (MMRs) with Jupiter. This is also the case of the Eos family, which is bracketed by the 7/3 MMR and intercepted by the 9/4 MMR (Fig. 2), just to mention the most powerful ones. With an increased number of members, Morbidelli et al. discovered more puzzling facts about this unusual asteroid family. In particular, they suggested the family seems to terminate at the 7/3 MMR at small values of semimajor axis and it is cut by the 9/4 MMR into two incompatible parts. Analyzing the number of family members on both sides of the resonance they pointed out a significant deficiency of family members with the orbital semimajor axis larger than $\simeq 3.03$ AU (position of the resonance). That was in odds with any reasonable initial velocity field of fragments from parent body break-up. A cascade of secondary fragmentations inside the original family was a possibility, but no other family showed indications of such process. On top of these findings Morbidelli et al. (1995) noted 5 asteroids associated with the family and residing inside the 9/4 MMR. By numerically integrating their orbits, they found instability occurs at a timescale of $100 - 200$ My with asteroids chaotically sliding along the whole resonance and ultimately ejected from the Solar system or hitting terrestrial planets. Morbidelli et al. hesitated to postulate that young age of the Eos family, leaning to the multi-break-up model. Nevertheless their work suggested a number of former Eos members might have escaped from the region of the Eos family along the 9/4 MMR toward orbits with significantly larger (or smaller) values of eccentricity and inclination. This prediction has been remarkably confirmed by the spectroscopic search reported by Zappalà et al. (2000) who observed 7 objects located inside the 9/4 MMR (but unrelated to the family with a simple clustering method in orbital element space). In the case of 5 of these asteroids they found spectra compatible with the Eos members, arguing thus these objects are very likely escaped, former members of the family and suggesting thus the Eos family actively feeds asteroids into the 9/4 resonance. Obviously, the issue of the family age cannot be solved with that observation, since we show below that the Yarkovsky-spreading model provides even more natural arena for feeding the resonance than the (multiple-)collision approach.[4]

Another approach to constrain age of an asteroid family is to analyze size-frequency distribution (SFD) and its evolution in time. An attempt to model this process has been performed by Marzari et al. (1995), who considered SFD evolution of the three most prominent families in the main belt: Themis, Koronis and Eos. While partially succeeding in the Themis and Koronis cases, the Eos family appeared unsatisfactorily matched by both SFD and orbital distribution modeling. As for the first issue, Marzari et al. (1995) –using mid 1990s state of art for the outcome of the collision breakup of large asteroids– obtained a mismatch with the observed family already in the initial SFD. This never improved, or got worse, letting the time go in their simulation. Reluctant to accept the very young age for the Eos family, Marzari et al. (1995) rather admitted a poor modeling in this case. This was even strengthened with their inability to match the anomalous orbital distribution in the proper element space (tight distribution in semimajor axis and larger dispersion in eccentricity and inclination), already pointed out by Brouwer (1951) and later confirmed by a number of analyses (e.g. Zappalà et al., 1984). We thus conclude that no satisfactory evolution model for Eos' SFD has been developed so far.

In what follows we show that many, though not all, puzzling facts about the Eos family are naturally solved in the framework coined by Bottke et al. (2001, 2002). In their point of view the asteroid families are originally more compact clusters in the proper element space than currently observed. Their initial compactness is assumed compatible with the numerical simulations of the asteroid catastrophic disruptions (e.g. Love and Ahrens, 1996; Ryan and Melosh, 1998; Benz and Asphaug, 1999; Michel et al., 2001, 2002), which

[4]Note the estimated sizes of the 5 fugitive asteroids from the Eos family located inside the 9/4 MMR range from 14 to 30 km. The likelihood, that they have been collisionally injected to the resonance from the neighborhood regions from family progenitors within the last $100 - 200$ My is minuscule.

means the observed fragments with sizes larger than few kilometres are ejected at relative velocity smaller than $\simeq$ 100 m/s. As time proceeds, the family undergoes evolution by two processes: (i) *collisional*, so that asteroids roughly smaller than $\simeq$ 10 km might suffer catastrophic disruption within a few Gy, producing secondary fragments populating the presently observed family, and (ii) *dynamical*, so that all proper elements[5] evolve due to chaotic diffusion in weak MMRs and thermal (Yarkovsky) forces making the initial cluster expanding in proper element space. The first aging mechanism has been appreciated and studied for a long time, but the second got increasing support only in the late 1990s.

The evidence of an overall chaoticity of the asteroid motion due to the effect of weak MMRs has been provided by series of papers during the early 1990s (as an example see Milani and Nobili, 1992; Milani and Farinella, 1994; Milani et al., 1997). Nesvorný and Morbidelli (1998), and Morbidelli and Nesvorný (1999), came with a thorough analysis of a very long-term orbital evolution of the main belt asteroids and suggested the numerous weak (high-order or multiple) resonances drive overall instability. This causes virtually all orbits, especially in the inner and outer parts of the belt, to evolve in time. In particular, orbital eccentricity and inclination are changing due to these resonant perturbations. The bodies may be thus driven to planet-crossing orbits (Morbidelli and Nesvorný, 1999) and escape from the main asteroid belt. A less spectacular effect is a smearing any compact structures in the main belt along the eccentricity and inclination direction, a process important for the asteroid families. For instance, Nesvorný et al. (2002a) have shown that the chaotic evolution in the inner part of the main belt (the Flora zone) is so intense that an initially compact Flora cluster would disperse to its current extent in 0.5 Gy only.

The second dispersal mechanism of the asteroid families is due to thermal (Yarkovsky) forces. They cause, on a long-term, a steady change in semimajor axis as a function of size, thermal parameters and rotation state (the obliquity and rotation rate, in particular; for a review see Bottke et al., 2002). Farinella and Vokrouhlický (1999) suggested asteroid families might undergo non-negligible evolution due to the Yarkovsky effect, namely spreading small members over a larger interval of semimajor axes than large members as time proceeds. Over the few last years, this idea got a solid support along different lines of evidence.

Bottke et al. (2001) proved the Koronis family undergoes a steady dispersion in semimajor axis by explaining a long-standing problem of the "Prometheus clan", a part of the family at its large semimajor axis end which is, as a whole, lifted by $\simeq 0.025$ in proper eccentricity. No reasonable velocity field could have explained this feature (e.g. Marzari et al., 1995). Yet, it appears natural in the new scenario, because Bottke et al. (2001) showed that orbits migrating from the centre of the family toward larger semimajor axis values encounter a high-order secular resonance $g + 2g_5 - 3g_6$ (e.g. Milani and Knežević 1990, 1992, 1994). Interaction with this resonance necessarily leads to the observed eccentricity increase, and the required drift rate of the semimajor axis is well compatible with the Yarkovsky effect prediction.

More recently, Nesvorný and Bottke (2004) studied young (5.8 My old) Karin cluster in detail and showed that convergence of orbits into a single original configuration is much improved if semimajor axis of Karin members has been steadily changing in time and in a way compatible with the Yarkovsky effect prediction. This again is practically a proof of the Yarkovsky-driven dispersion of the Karin cluster that was detected amazingly soon after the family formation.

A little less direct, yet convincing, evidence of the Yarkovsky dispersion of Koronis and Eos families was obtained by Tsiganis et al. (2003). These authors studied a population of asteroids residing inside the 7/3 MMR and proved one can consider it a steady-state population, continuously resupplied from outside the resonance. The pace at which this process works is well compatible with Yarkovsky delivery of asteroids into this resonance.

This model also predicts an asteroid population residing very closely to MMRs so that their orbits have a limited lifetime. Indeed, it has been

[5]The proper orbital elements have thus a time-local meaning, usually well characterizing orbital parameters over $\leq$ 10 My (e.g. Knežević and Milani, 2000, 2003). This timescale is often orders of magnitude less than the estimated age of the asteroid families.

known for some time that asteroid (2953) Vysheslavia has a very short dynamical lifetime as compared to the estimated age of Koronis family (e.g. Milani and Farinella, 1995). Vokrouhlický et al. (2001) suggested that the Yarkovsky forces are efficient enough to transport Vysheslavia from inside the Koronis family onto its current unstable orbit within $0.5 - 1$ Gy a comfortably short timescale. Additional work on Yarkovsky dispersion of the asteroid families has been done by Carruba et al. (2003) who suggested a comparatively young age of the Adeona and Gefion families.

Continuing the above work we bring here arguments that the Eos family must have undergone a substantial evolution due to the Yarkovsky effect in the past. This is because our model explains several observed features of this family that are otherwise puzzling or anomalous in context of other models. We start in Sec. 2 with reviewing fundamental facts about the Eos family, such as its structure in the proper element space, size-frequency distribution or spectral properties. In Sec. 3 we comment on anomalous features of the family and prove these are easily understood within the Yarkovsky-dispersion model. This is done using a numerical integration of a synthetic family and comparing its fundamental features to the real family. This model also brings some testable predictions, such as interloper asteroids inside the family. We observed spectra of several of these objects. Their reported spectral types are either compatible or incompatible with the Eos family members in a way that confirms our predictions.

2. Eos family: basic facts

In this section, we bring together fundamental properties of the Eos family as known today. First we apply formal clustering method on the most updated database of asteroids to identify the Eos family in the orbital element space. This significantly boosts number of asteroids associated with the family as compared to previous searches (e.g. Bendjoya and Zappalà, 2002), in particular extending information about the family toward its small members.[6] Second, we collect available spectral information about the identified members of the family (e.g. Cellino et al., 2002 and references therein).

2.1. Identification in the proper element space

We apply hierarchical clustering method (HCM; e.g. Bendjoya and Zappalà, 2002 and references therein) to identify members of the Eos family as a tight cloud of asteroids in the space of proper elements: semimajor axis a, eccentricity e and sine of inclination $\sin I$. We use analytically determined proper elements of nearly 170,000 main belt numbered and multi-opposition asteroids from `AstDyS` database (`http://newton.dm.unipi.it/`) as of November 2004. We tested different values of the cut-off velocity $V_{\rm c}$ in between 30 m/s and 85 m/s which is the principal free parameter in the HCM method. (In fact only values larger than $\simeq 30$ m/s have a good sense because the intrinsic noise of analytical proper elements is of this order of magnitude.) At the largest tested values the cluster starts to accumulate a large portion of the surrounding region in the proper element space. This is seen in Fig. 1 where we show number of HCM identified members of the neighboring Eos and Veritas families as a function of $V_{\rm c}$. At the critical value $V_{\rm c} = 78$ m/s, with our catalogue, the two families coalesce into a single global cluster of asteroids. This plot also nicely shows intrinsic difficulty of family identification in case of the large families like Eos. The compact (and young; e.g. Nesvorný et al., 2003) Veritas family depends very weakly on $V_{\rm c}$ until the moment it collapses with nearly the whole background field of asteroids, so that it is defined very distinctly.[7] Conversely, in the Eos case increasing the $V_{\rm c}$ means to steadily increase number of associated asteroids. This process certainly results in an accumulation of interloper objects from some value of $V_{\rm c}$ with only a loosely defined strategy to eliminate them with the formal clustering method. Trials and tests are needed at this stage of work.

Figure 2 shows two examples of the Eos family identification for $V_{\rm c} = 50$ m/s (left) and 55 m/s (right; dots are background main belt asteroids inside a orbital-element box defined by

[6] The last searches of Nesvorný et al. (2005a) and Monthé-Diniz et al. (2005) used proper element catalogues containing only about half objects.

[7] The same concept may be also nicely seen using the stalactite diagram shown in Fig. 4 of Nesvorný et al. (2005a).

the ranges of the axes). The family identification at different values of V_c is made available at our web-site `http://sirrah.troja.mff.cuni.cz/yarko-site/`. The case $V_c = 55$ m/s appears to us a good and still conservative compromise between completeness and overshooting; at larger V_c values the family basically starts to accumulate more and more distant asteroids with semimajor axis larger than $\simeq 3.03$ AU, i.e. above the 9/4 MMR with Jupiter. In what follows we thus use this choice as a nominal definition of the Eos family. Figure 3 shows the Eos family projected onto the plane of proper semimajor axis a and absolute magnitude H (data are taken consistently from `AstDyS` web-site) again for the two V_c values. We shall discuss outstanding and peculiar features of the family structure, shown in these two figures, in Sec. 3.

In fact, any of 2-D projections shown in Fig. 2 misses to show in detail full structure of the family in the three-dimensional space of proper orbital elements. In Fig. 4 we thus show the Eos family as a 3-D cluster (bold symbols) embedded in the background population of asteroids (dots). The chosen view puts emphasis on low-eccentricity and low-inclination side where one can notice a stream-like structure radiating out of the family (on our website `http://sirrah.troja.mff.cuni.cz/yarko-site/` we provide a computer animation that allows to see the Eos family from many different directions in the proper element space). The two planes shown in the same figure roughly delimit libration zone of the high-order secular resonance z_1 (e.g. Milani and Knežević 1990, 1992, 1994, and Sec. 3.3). We notice the peculiar structure observed in the family tightly adheres to this resonance. In Sec. 3.3 we explain this peculiarity.

We also investigated cumulative distribution $N(< H)$ of absolute magnitudes H for Eos family asteroids. This can be achieved with high reliability, since even with low V_c values the family contains thousands of members; in particular, the nominal family with $V_c = 55$ m/s has about 4400 asteroids. Figure 5 shows this quantity for the three velocity cut-off values – 50 m/s, 55 m/s and 60 m/s. We used a power-law approximation $N(< H) \propto 10^{\gamma H}$ in the magnitude range $(11.5, 13.5)$ and obtained $\gamma \simeq 0.47 \pm 0.02$ for the nominal family at $V_c = 55$ m/s. Our value of γ is close to some previously reported values (e.g. Fujiwara, 1982), but discordant with some others (e.g. Tanga et al. (1999) who predict a considerably steeper distribution from their geometric method). This value of the power index suggests that at small size the family has undergone collisional evolution that drove it toward the equilibrium state (e.g. Dohnanyi, 1969; O'Brien and Greenberg, 2003) and it argues for a significant age of this family. In particular, Bottke et al. (2005a,b) estimate a $15 - 20$ km size asteroid (roughly the absolute magnitude 11.5 for the Eos case) has a collisional lifetime of $\simeq 2$ Gy; thus we would tentatively infer and age of $1-2$ Gy from this simple argument. Interestingly, our more quantitative work in Sec. 3.2 will confirm this age rather well.

Another interesting result in shown in Fig. 6 where we give the best approximating power-index γ in the magnitude range $(11.5, 13.5)$ as a function of the cut-off velocity V_c. Except the anomalous "step" at $V_c = 44$ m/s which is caused by a sudden extension of the family to the region beyond the 9/4 mean motion resonance with Jupiter (see also Fig. 1), the fitted power-index γ steadily increases. The limiting value $\simeq 0.52$ can be attributed to the overall main-belt population of asteroids in this particular heliocentric zone since at larger value of V_c the family fills basically the whole surrounding region. The fact that at any smaller V_c value the family is shallower is interesting and fits the finding by Morbidelli et al. (2003) about comparative shallowness of the asteroid families.

2.2. Spectroscopic observations

Information about the physical properties of the Eos family members derives from spectroscopy of large asteroids and Sloan Digital Sky Survey (SDSS) broad-band photometry of small asteroids. Here we give some basic information about both sources.

We start with results from spectroscopic surveys. There are, though, at least two reasons of caution that must be taken into account when trying to compare data from different sources: (i) taxonomic systems significantly evolved over the past two decades, and (ii) major surveys used spectroscopy in visible band only. This later point places an important constraint, because fine discrimination of physical properties (especially for an object at the outskirt of the broad S-complex)

requires additional data in the infrared. This has been actually the case of (221) Eos itself, and several other largest Eos members, whose visual spectra resemble S-type objects (apart from finer details introduced only later on). It was only when an extended spectrum of (221) Eos, covering both visual and infrared bands, was first obtained, within the 52-color survey that Bell et al. (1987) and Bell (1989) discriminated its spectrum from an S type and proposed to introduce a new spectral class: K type. As Bell (1989) rightly points out, the case of Eos presents an apparently contradictory situation when broad-band photometry originally led to a common wisdom of homogeneity inside family members but the spectroscopy often had problems in a tight and clear spectral classification. However, we do not intend to overview history of different views on Eos-type spectra and refer to Veeder et al. (1995) and Doressoundiram et al. (1998) for reviews.

Migliorini et al. (1995) conclude, from an unrelated-to-spectroscopy statistical argument, that a few interlopers are expected at all sizes. Indeed, a dedicated visual spectroscopic survey of large Eos members by Doressoundiram et al. (1998) confirms two interlopers (1910) Mikkailov and (4455) Ruriko spectrally similar to C-type asteroids, in a sample of 45 observed family members.[8] Additionally, this important study confirmed an earlier suggestion by Xu et al. (1995) of a modest spectral heterogeneity of the Eos members, ranging from the K types, such as (221) Eos itself, to T types. Both these classes are situated at the edge of the S-type complex consistently along the line toward a flatter long-wave end of the spectrum, thus more neutral value of the PC2 components, with approximately the same slope parameter (Bus and Binzel, 2002a,b). As mentioned above, this borderline position of the Eos-members spectral types makes it sometimes a bit difficult to be unambiguously classified. For instance, out of the 45 asteroids observed by Doressoundiram et al. (1998) we can find 6 included in the SMASSII catalogue (Bus and Binzel, 2002b). In their taxonomic system, 4 were classified K type while 2 got S type classification: (633) Zelima and (1186) Turnera. The spectral differences reported by Doressoundiram et al. (1998) has been interpreted by these authors as some kind of weathering process effective in the family or perhaps compositional differences in the Eos parent body. However, up to our knowledge there is no general consensus about this interpretation as yet.

We also note that SMASSII survey detected 19 asteroids that are associated with the Eos family at the HCM cut-off velocity $V_c = 55$ m/s (Bus and Binzel, 2002a,b; see also updates at `http://smass.mit.edu/`). Most of them got K type classification, with the exception of the two S type asteroids mentioned above, and two interloper asteroids: (1604) Tombaugh and (3214) Makarenko both classified to be Xc-type asteroids. This again seems to confirm a low rate of interloper contamination within the Eos family.

Another wealthy and recent source of spectroscopic data is the S^3OS^2 survey by Lazzaro et al. (2004) (see `http://www.daf.on.br/~lazzaro/S3OS2-Pub/s3os2.htm`). In total this survey observed 13 asteroids from our nominal Eos family with the following result. Asteroids (1075) Helina (Xc-type), (1605) Milankovitch (X-type), (3328) Interposita (Xc-type), and (4100) Sumiko (B-type) are all spectrally diverse from prevalent K and T types in the Eos family and contribute to the interloper population. Asteroids (251) Sophia (Sl-type) and (4843) Megantic (X-type) are also recognized as interlopers. Moreover, several asteroids were re-classified as D types within the new Bus taxonomy from former T types of Tholen taxonomy, confirming difficulties in spectral classification.

Both datasets, SMASS and S^3OS^2, have been compiled together and applied systematically to the asteroid families by Monthé-Diniz et al. (2005). For the Eos family, likely identified by these authors at a slightly larger relative HCM cutoff, they determined that 55 out of 92 asteroids with known spectra belong to the KTD sequence, thus forming a backbone of the family classification. It is, however, worth to recall that the mineralogical interpretation of these data remain puzzling (e.g. D types here often have high albedo value, unlike the well interpreted low-albedo D type objects in the outer part of the asteroid belt and among Trojan asteroids). With Xk types, related in optical band, the KTD's form

[8] We note, though, that (1910) Mikkailov associates with the family only at the HCM cut-off velocity $V_c = 60$ m/s and thus is not a member of our nominal Eos family defined at $V_c = 55$ m/s.

74% of family asteroids. Alien, or more distant spectral types (X, C and B) constitute some 26% of asteroids in the Eos family somewhat more than previously expected (Migliorini et al., 1995). Their fraction increases with larger velocity cut-off values, suggesting the family is embedded in a spectrally alien zone. In spite of not well understood compositional implications of the KTD spectral sequence inside Eos family, the primitive types may give a partial chance to recognize interloper objects.

As far as broad-band photometry is concerned, we skip the older observations in the Johnson UBV system (e.g. Zellner et al., 1985), and we note a more recent work of Ivezić et al. (2001, 2002) who analyzed homogeneity of asteroid families using the broad-band 5-color data of SDSS (see `http://www.astro.princeton.edu/~ivezic/sdssmoc/sdssmoc.html`). Interestingly, in the case of Eos they conclude a slight scatter of spectral indeces which makes the family not very compact in space of the SDSS spectral parameters (though these authors do not analyse the Eos family in detail). Since the SDSS data are available mostly for small asteroids ($H \geq 12$, say), the result of Ivezić et al. might indicate spectral heterogeneity in the Eosfamily, concluded by Doressoundiram et al. (1998) and followers, continues at small sizes too. A more thorough analysis of a release 2.0 SDSS data has been given by Nesvorný et al. (2005a), whose primary focus was to study the space weathering effects using asteroid families data. For Eos, these authors were able to identify SDSS colors for 457 members, though their identification used somewhat larger velocity cut-off than our nominal family (thus likely containing more interloper asteroids). Their average principal component values found for Eos members were $\mathrm{PC}_1 = 0.466 \pm 0.095$ and $\mathrm{PC}_2 = -0.104 \pm 0.083$ (standard deviations), placing this family rightly at the outskirt of the S-complex. That borderline position complicates interpretations, but extreme locations of some objects may help identification of the interlopers within the family (see Sec. 3.4).

Additional possible interlopers inside the family, suggested by the infrared broad-band photometry reported by Veeder et al. (1995), are (562) Saloma and (1723) Klemola, whose J-H color index is significantly offset from other observed members of the family. Some authors, e.g. Bell (1989), suspect the third largest asteroid associated with Eos family, (639) Latona, might be an interloper based on S-like behavior of in the infrared band.

In Sec. 3.4 we report additional spectral observations of the Eos members we made over past few years. Most of them were motivated to confirm our model of expanding family to verify guessed interloper asteroids or to confirm possible members at the outskirt regions of the family. We also analyze the most updated SDSS data, release 3.0.

3. Eos family: Yarkovsky traces

Hereafter we analyze several outstanding features of the Eos family and we show they make a good sense only in the dynamical model, where the family has been formed more compact in the proper element space about a Gy ago and since then it underwent a significant dispersion by the two processes discussed in Sec. 1. To that end we first perform a numerical simulation to see how an initially compact cluster near the centre of the Eos family extends in the proper element space in course of time. The initial data we use are certainly simplified since they do not follow from any sophisticated simulation of a collisional disruption of an asteroid (such as hydrocode modeling). However, we argue this is not really a fundamental issue as long as they are compatible with reality in the most important parameter for us: the low mean velocity with which sizable fragments are dispersed (e.g. Love and Ahrens, 1996; Ryan and Melosh, 1998). The main point of our simulation is to see the effects of dispersal mechanisms on the family structure. These effects are actually so overwhelming the current structure of the family that no attempt to deterministically reconstruct the initial family configuration in the proper elements space is possible.

Thus to set the initial orbital elements of the synthetic family asteroids we use the procedure described in the Appendix of Carruba et al. (2003). In the Eos case, the estimated mass ratio of the largest fragment and the parent body is $\simeq 0.1$ (e.g. Tanga et al., 1999; Campo Bagatin and Petit, 2001). Using this value we obtain a parent body of $D_{\mathrm{PB}} \simeq 240$ km size. A specific energy $Q_D^\star$ to collisionally disrupt this object is estimated using results of Benz and Asphaug (1999): $Q_D^\star \simeq 0.1\,\rho\, D_{\mathrm{PB}}^{1.36}$ where we set $\rho \simeq 2.5$ g/cm^3 for

bulk density. Only a small part of this energy is transformed into kinetic energy of dispersed fragments, such that their mean quadratic velocity $v_{\rm ej}$ is $v_{\rm ej}^2 = 2\, f_{KE}\, Q_D^\star$ (e.g. Davis et al., 1989, Petit and Farinella, 1993). The fundamental anelasticity parameter $f_{KE} \simeq 0.02$ is intentionally chosen small, such that $v_{\rm ej}$ becomes tens of m/s only. Following the work of Petit and Farinella (1993) we also correct for self-gravity of the parent body, so that the escaping fragments must have a positive value of binding energy. We also assume $v_{\rm ej}$ have Maxwellian distribution and, for simplicity, no mass/size dependence of $v_{\rm ej}$ is taken into account (certainly valid only in some limited size range). The initial velocity field is isotropic in space (below we shall argue that this is probably the most unrealistic assumption, as regards the properties of the true initial data of this family). Finally, we transform the initial velocity field into orbital element dispersion using Gauss equations and the parent body true anomaly f and argument of pericenter ω such that: $f = 90^\circ$ and $\omega + f = 45^\circ$ (see e.g. Morbidelli et al., 1995).

We use a SWIFT-RMVS3 integrator (e.g. Levison and Duncan, 1994) modified to account for the Yarkovsky forces (see `http://sirrah.troja.mff.cuni.cz/yarko-site/` for details of its implementation, speed and accuracy tests). We also complemented the original version of the integrator with computation of synthetic proper elements in a way compatible with a definition of Knežević and Milani (2000, 2003). This means that we first apply a Fourier filter to the (non-singular) orbital elements in a moving window of $\simeq 0.7$ My (with steps of 0.1 My) to eliminate all periods smaller than some threshold (1.5 ky in our case; we use a standard sequence of Kaiser windows as in Quinn et al., 1991, a procedure equivalent to what is used by Knežević and Milani, 2000). The filtered signal, mean orbital elements, is output from the simulation for further checks and passed through a frequency analysis code adapted from Šidlichovský and Nesvorný (1997) to obtain (planetary) forced and free terms in Fourier representation of the orbital elements. The isolated free terms are what we use as the proper orbital elements.

Giant planets are included in our simulation with their masses, initial positions and velocities taken from the `JPL DE405` ephemeris. The effect of the terrestrial planets accounted for as a barycentric correction of the initial conditions only, which is fairly justified in this zone of the asteroid belt. A timestep of 20 days is used. For sake of our test, we use 210 test particles (asteroids) with their initial orbits generated by the above described scheme. Their sizes range from 2 km to 60 km; smaller bodies dominate in our integrated sample such that we have 10 bodies of 60 km size in our sample and there are $\propto 1/D$ bodies in different size bins.[9] Distribution of their rotation rate is set Maxwellian with a peak value corresponding to a period of 8 hr (though we prevent shorter/longer periods than 4/12 hr; e.g. Binzel, 1988) and orientation of spin axis is uniform in space. Since our numerical simulation is an illustration of principles, we allow ourselves to keep rotation parameters for each of the asteroids (rotation period and spin axis orientation) constant. This is a gross simplification, since on a Gy timescale thermal and gravitational torques produce large variations of both rotation parameters (see e.g. Sec. 3.2). But here we waive complexity for simplicity. Obviously, conclusions from our results should then be treated with caution. Thermal parameters, necessary for modeling Yarkovsky forces, are: thermal conductivity $K = 0.005$ W/m/K, specific heat capacity $C_p = 680$ J/kg/K, surface and bulk densities 1.5 and 2.5 g/cm^3. This is about the best guess we can do for multikilometre asteroids in the Eos region which likely have an insulating surface layer of dust or at least significant porosity (making K small). We use analytic formulæ of Vokrouhlický (1998, 1999) and Vokrouhlický and Farinella (1999; Appendix) for both diurnal and seasonal variants of the Yarkovsky effect. With the chosen thermal parameters the diurnal effect is about an order of magnitude larger than the seasonal effect, producing thus both inward and outward migration of asteroids wrt the Sun.

After setting initial conditions and thermal parameters, we let our synthetic family evolve for 1 Gy (this end-time is chosen in a rough accordance with our estimate of the family age in Sec. 3.2). Figures 7 and 8 show evolution of the proper elements –semimajor axis, eccentricity and inclination– in course of time (solid lines), superimposed onto positions of the currently observed

[9] In fact, we use 8 size bins in logarithmic measure and set a uniform number of objects in each of them.

Eos family members (dots). The former figure tracks evolution of asteroids with size $D \geq 7$ km, while the latter is for asteroids with size $D \leq 7$ km. In both figures we show position of major MMRs –7/3, 9/4 and 11/5– as well as numerous weaker MMRs such as high-order resonances (e.g. 16/7 or 23/10) and three-body resonances with Jupiter and Saturn (e.g. 8J−3S−3, 6J+2S−1, 5J−1S−2 or 3J−2S−1[10]; Nesvorný and Morbidelli, 1998; Morbidelli and Nesvorný 1999; Morbidelli 2002).

The effect of resonances on orbits migrating in semimajor axis is twofold, depending of the strength of the resonance and rate of the drift.

The weak resonances can temporarily capture an orbit and make its proper eccentricity e and/or inclination I changed by a small amount upon leaving the resonance (Fig. 9; see also Vokrouhlický and Brož, 2002). The effect is not able to force asteroids to leave the family in this zone of the asteroid belt, but large enough to make the mean dispersion in e and I increased in time. Our simulation suggests that this effect is virtually able to build the full eccentricity extent of the family, but not the inclination extent where it misses about a factor of two. However we remind, our integrations assumed for simplicity fixed orientation of spin axis in space for each of the test particles, while thermal and gravitational torques, together with collisional effects, may result in its complicated evolution. As a response to this spin axis evolution, the drift rate at which Yarkovsky forces change semimajor axis could change, or even reverse, in time, making thus to cross the weak resonances at variable speed of from different directions. This could help increasing dispersal effect of weak resonances in e and I to an unknown extent, whose complete numerical simulation is beyond the scope of this work. We also remind, that our isotropic initial velocity field was unrealistic enough to assume some part of the "inclination problem" might go into a possible larger initial inclination spread due to its anisotropy (Sec. 4).

Principal MMRs, 7/3, 9/4 and even 11/5, have a power to eliminate particles from the family by significantly increasing (or decreasing) eccentricity and/or inclination upon capture. The strength of the effect is proportional to the order of the resonance (e.g. Morbidelli, 2002), but it also depends on rate by which Yarkovsky forces push the semimajor axis. In Eos we have a very interesting situation, since the effect of principal MMRs ranges from near total elimination of the observable particles (7/3 MMR) to their partial elimination (9/4 MMR). Both produce quantitatively testable effects: termination of the family in the former case and a rate-dependent drop in semimajor axis density of asteroids after passage of the latter. We devote Section 3.1 to a careful study of this effect and its comparison with the observed data.

Figure 10 shows a zoom into interaction zone of the Yarkovsky drifting orbits with the J11/5 and 3J−2S−1 resonances. This doublet is close enough to cause partial elimination of bodies from the family. This is mainly happening for orbits reaching the J11/5 resonance at an eccentricity "pumped up" by a previous interaction with the J9/4 resonance. The chance to cross this doublet is better at lower eccentricity and indeed a look at Fig. 2, HCM 55 m/s, we note the family first extends beyond the J11/5 and 3J−2S−1 resonances at the lowest values of e.

The last resonant effect, very specific to the Eos family, is the influence of the high-order secular resonance z_1 (e.g. Milani and Knežević, 1990, 1992, 1994). We shall describe it in full detail in Sec. 3.3, here it is sufficient to note that many asteroids in our simulation follow a "diagonal route" toward smaller values of proper eccentricity and inclination. At the same time, location in this resonance makes the proper e and I to oscillate with a rather large amplitude and a period of several My. Asteroids migrating toward large value of the semimajor axis may also follow this secular resonance, but the 9/4 MMR presents an obstacle that efficiently removes bodies from the family (and the z_1 resonance at least).

With the above numerical simulation as a toy example, we are now ready to discuss some particular and interesting features in the structure of the Eos family in more detail.

3.1. 7/3 and 9/4 MMR tests

Sharp termination by the 7/3 MMR (Figs. 2 and 3) is among the most astonishing properties

[10] We adopt the notation of Nesvorný and Morbidelli (1998) and Morbidelli (2002) who characterize a three-body MMR ($+m_J$J$+m_S$S$+m$) with a condition $m_J\dot{\lambda}_J+m_S\dot{\lambda}_S+m\dot{\lambda} \simeq 0$, where λ_J, λ_S and λ are mean longitudes of Jupiter, Saturn and the asteroid.

of the Eos family.[11] We note that the width of 7/3 MMR, at the mean eccentricity value of the Eos orbits, is $(\Delta a)_{7/3} \simeq 7 \times 10^{-3}$ AU. This value can be approximately interpreted in terms of a HCM velocity distance $(\Delta v)_{7/3}$ as $(\Delta a)_{7/3}/a_{7/3} \simeq (\Delta v)_{7/3}/v_{7/3}$; here $a_{7/3}$ is the position of the resonance and $v_{7/3}$ is the characteristic orbital velocity at the resonance. With this relation that assumes no difference in eccentricity and inclination, we estimate the 7/3 MMR presents an "obstacle" of $(\Delta v)_{7/3} \simeq 10$ m/s in the HCM scheme. This estimate has been obtained using a circular three-body problem and thus the true width of the 7/3 resonance might be little larger, but it seems that using the cut-off limit of 55 m/s, as in the case of our nominal family, we should be able to easily link a tail of the family extending beyond the 7/3 MMR if it existed with a comparable asteroid density as above the 7/3 MMR. In fact, only a few asteroids get associated with the family beyond the 7/3 MMR even at HCM cut-off velocity $V_{\rm c} = 70$ m/s, and these likely represent the background population of objects (anyway associated with the family at this large $V_{\rm c}$ in great number; Sec. 2) or just a few Eos escapees through the resonance (e.g. Fig. 8). We thus conclude that the Eos family does not extend beyond the 7/3 MMR, even though it tightly adheres to it along a significant interval of eccentricity and inclination values. We cannot imagine this observation can make any sense if we wanted to interpret the current family configuration in terms of the initial velocity field (such as in Zappalà et al., 1996, or Cellino et al., 1999). Rather, we conclude the initial family was barely reaching the 7/3 MMR border and there has been a continuous flow of Eos members toward this resonance since then. Asteroids reaching the resonance were presumably eliminated by the chaotic evolution inside (e.g. Tsiganis et al., 2003), either were not permitted to pass through the resonance or upon passing it they reached significantly different values of eccentricity and inclination. Our expanding-family model fully entails this idea and thus directly explains this, otherwise puzzling, feature.

[11] We note, though, it is not unique among other families: Koronis family shows the same termination by the 5/2 and 7/3 MMRs (e.g. Bottke et al., 2001), Eunomia family by the 3/1 MMR (e.g. Morbidelli and Vokrouhlický, 2003), as well as several other families (e.g. Morbidelli et al., 1995).

However, to proof our claim is correct, we must perform a quantitative test. Note few of the integrated small-size objects in our previous section succeeded to cross the 7/3 MMR and continue drifting to smaller semimajor axis. This is because probability to cross the resonance depends on the drift-rate in semimajor axis and the small bodies eventually drift fast enough to cross the resonance. (Note this phenomenon is well known from planetary dust studies, where small particles, up to tens of microns in size, efficiently cross any of principal resonances in the main belt, but larger particles, from few hundred microns in size, are scattered by these resonances; e.g. Dermott et al., 2001; Nesvorný et al., 2005b). In what follows, we thus study this crossing probability for Yarkovsky drifting orbits using numerical integration. Each time we take a sample of 102 asteroids of a given size initially located above the 7/3 MMR and we let them drifting by the Yarkovsky forces toward the resonance. We used osculating orbital elements of real Eos members located close to the 7/3 MMR as the initial data. To make the effect statistically average for a given size, we fix the obliquity to 135° for each of the particles. Other thermal parameters and rotation rate are as in our previous numerical simulation of the overall family expansion. We investigate five characteristic sizes corresponding to the absolute magnitudes $H = 13, 14, 15$ and 16 (we use the mean albedo $p_V = 0.13$ for the size-magnitude conversion). The smallest chosen magnitude marks approximately the limiting value at which the family members adhere to the 7/3 MMR (see Fig. 3).

Table 1 summarizes the results of our experiment. In general only the smallest asteroids with the initially low eccentricity and inclination were able to cross the 7/3 MMR. Among the $H = 16$ mag, thus $D \simeq 2.4$ km, bodies we recorded 13 such cases. We thus conclude that a few km-sized asteroids beyond the 7/3 MMR might be Eos escapees. Provenience of these putative objects would be the small e and I tail of the Eos family which is itself not densely populated (bulk of the family members have $e \geq 0.07$ for which we did not recorded crossings of the 7/3 MMR). However, these smallest bodies are hardly observed at the distance of Eos family (see Fig. 3) and the first statistically well populated bin is that of $H = 15$ mag. Very few of these larger objects manage to cross the 7/3

MMR though. It is then not surprising, that the Eos family does not extend beyond this powerful resonance.

The case of the 9/4 MMR is even more interesting than the 7/3 MMR, since it permits more quantitative testing of our Yarkovsky-flow model. This is because the 9/4 MMR is weaker and thus allows more drifting orbits to cross it. On the the other hand, it is still powerful enough to eliminate some part of the captured orbits. The characteristic ratio of eliminated/crossing orbits may be readily compared with the population of Eos members of a given size, on both sides of the 9/4 MMR. To provide this comparison, we again first integrated a large number of orbits, corresponding to bodies of a given size, and let them reach the 9/4 MMR. We thus took groups of 106 particles with absolute magnitudes $H = 10 - 16$ and assigned them the same thermal and physical parameters as above. We used osculating orbital elements of real Eos members with proper $a \in (3.023, 3.027)$ AU, i.e. below the 9/4 MMR, as the initial conditions. In this case, we chose obliquity to be 45° to let the orbits migrate toward large values of the semimajor axis.

Table 2 gives our results. As expected, significantly more asteroids, as compared to the 7/3 case, crossed this higher order resonance.

A quantitative comparison of the probabilities to cross the 9/4 MMR from the Table 2 to the data of the observed family needs additional assumptions, since they cannot be directly linked to the number of asteroids of a given magnitude/size on both sides of the resonance. This is because of two reasons. First, the 9/4 MMR is miscentered in the family, for its position at $a_{9/4} \simeq 3.03$ AU is to be compared with the family center at $a_c \simeq 3.02$ AU. Thus, there is a priori bias to have more Eos members below the 9/4 than above and we have to correct for this effect. Second, the left side of the family is cut by the J7/3 resonance. As a result, distribution of asteroids with $a \leq a_c$ gives us only a limited information not extending below $a_{7/3} \simeq 2.957$ AU. Our procedure is as follows.

Focusing, at first, on the Eos region that corresponds to $a \leq a_c$ we denote $\mathcal{B}(a; H)$ density distribution of members with absolute magnitude H. Thus

$$\mathcal{B}(a; H) = \frac{dN}{da} \,, \qquad (1)$$

where dN is number of Eos members in the semimajor axis interval $(a, a+da)$ with $a \leq a_c$ and having absolute magnitude is some small range about H. The zone $a \geq a_c$ has been presumably affected by the 9/4 resonance in course of time evolution, but we find admissible approximation (though not necessarily true) that the initial distribution of Eos members has been symmetric about a_c. Assuming the evolution processes would not violate this postulated initial symmetry, we expect

$$N^{<}_{\rm exp}(H) = \int_{a_{7/3}}^{a_{9/4}} \mathcal{B}(a; H)\, da \qquad (2)$$

asteroids of absolute magnitude H to reside in the Eos family on the left hand side of 9/4 MMR (note the family extends to the 7/3 MMR only, thus the lower semimajor axis value is set to the location of this resonance) and

$$N^{>}_{\rm exp}(H) = \int_{a_{9/4}}^{2a_c - a_{7/3}} \mathcal{B}(a; H)\, da \qquad (3)$$

asteroids of absolute magnitude H to reside in the Eos family on the right hand side of 9/4 MMR (we also assume here $\mathcal{B}(a; H) = \mathcal{B}(2a_c - a; H)$ which expresses symmetry of the $\mathcal{B}$-function about a_c). Denoting $N^{<}_{\rm obs}(H)$ and $N^{>}_{\rm obs}(H)$ the numbers of truly observed family members below and above the 9/4 MMR, we finally define

$$r(H) = \frac{N^{>}_{\rm obs}(H)/N^{>}_{\rm exp}(H)}{N^{<}_{\rm obs}(H)/N^{<}_{\rm exp}(H)} \,. \qquad (4)$$

The value of $r(H)$ is a measure of how the true Eos population follows assumptions of equal dispersion/evolution of the family toward smaller and larger semimajor axis value. In particular, if $r \simeq 1$ they are well satisfied.

Figure 11 shows the ratio $r(H)$ for the Eos family identified with three HCM velocity cut-offs: 50 m/s, 55 m/s (nominal value; thin line) and 60 m/s. The fact that $r(H)$ is always smaller then unity quantitatively confirms that there is a net depletion of the observed members in the Eos family on the right side of the 9/4 MMR. We also note, that $r(H)$ is strongly size dependent, making the relative paucity of Eos members beyond the 9/4 MMR larger for larger asteroids.

This observation is as such surprising in the frame of a static model, where the Eos family

would not dynamically evolve (see the discussion in Morbidelli et al., 1995). In our scenario, the fact becomes natural, because the 9/4 MMR is expected to eliminate part of the Eos asteroids migrating toward larger a across the resonance. In fact, if our model would be perfectly correct, the $r(H)$ values should be equal to the probability $c(H)$ of crossing the 9/4 MMR with the Yarkovsky drifting orbits that we obtained from test integrations above (Table 2). For that purpose we plotted in Fig. 11 the crossing probability $c(H)$ together with $r(H)$.

We note a rough agreement of $r(H)$ and probability to cross the 9/4 MMR. In particular, both indicate no (or very few) bodies with $H \leq 10$ should cross the resonance. The principal difference though is seen in lower crossing probabilities in the $H = 12 - 14$ range. We can find several reasons for this mismatch:

- The exact match of $r(H)$ and the crossing probability inherently assumes all asteroids must once cross the resonance. However, our model in Sec. 3.2 indicates a small fraction of asteroids might be initially injected on the right hand size of the 9/4 MMR. The best fit solution predicts this happens for $H \geq 13$ and it may help increasing the local population of the Eos members with $a \geq a_{9/4}$.

- Asteroids below some size threshold might typically reach the 9/4 MMR with smaller obliquity and thus migrate faster (as if they had effectively smaller size in our simulation). This might be due to the YORP effect completing a cycle toward its asymptotic state within the estimated family age of slightly more than 1 Gy (Sec. 3.2). The work of Vokrouhlický et al. (2003), and previous theoretical studies, suggest $D \simeq (30-40)$ km Koronis asteroids complete the YORP cycle in about 2.5 Gy. Scaling appropriately this result, and using the mean albedo value $p_V \simeq 0.13$ for the Eos members, we would assume $H \geq 12$ mag asteroids are small enough ($D \leq 15$ km) to reach a near asymptotic YORP states within the necessary timescale. This would efficiently shift data points corresponding to $H \geq 12$ mag in Fig. 11 by about 0.75 magnitude toward smaller values, and also help bringing the $r(H)$ and $c(H)$ closer each other.

Thus, in spite of not perfect agreement we consider, given our above arguments, the result of our test satisfactory.

3.2. $a - H$ projection analysis

Like other families, the Eos family shows a typical pattern when its members are projected onto the plane defined by semimajor axis a and absolute magnitude H: the largest asteroid resides near the mean value of a for the family, while extreme values of a are occupied by the smallest asteroids only (Fig. 3). Because it appears natural that smaller fragments received larger relative velocity with respect to the parent body during the initial catastrophic disruption, Cellino et al. (1999) attempted to use this distribution of family members to calibrate the unknown velocity-size relation assuming families did not dynamically evolve in semimajor axes since their formation (this work followed an earlier study by Zappalà et al. (1996), except for recognizing that proper eccentricity and inclination might be unstable on a long-term due to effects of weak resonances). However, Bottke et al. (2001) pointed out an inadequacy of Cellino et al. (1999) model by not taking into account long-term spreading of the family in the semimajor axis direction due to the thermal forces. Thus only after including all these evolutionary processes one might attempt to reconstruct an approximate extension of the initial cluster of fragments and try to apply methods similar to those in Cellino et al. (1999) or Zappalà et al. (1996).

In what follows we use a simple model of Vokrouhlický et al. (2005) to show that the Eos family had originally semimajor axis extension equivalent to about $30 - 50\%$ of the currently observed family. The remaining part has been acquired later as a result of the dynamical dispersion due to the previously mentioned evolutionary processes. These results are in good agreement with an independent analysis of Dell'Oro et al. (2004), who suggest that the initial families were statistically smaller than the observed families by a factor of two. Our work is more quantitative and it allows also to approximately determine the age of the Eos family, extending and substantiating thus results from Nesvorný et al. (2005a).

3.2.1. Method

Here we briefly recall the method of Vokrouhlický et al. (2005) to analyse semimajor axis dispersion for an asteroid family. Consider a projection of the family members onto the (a, H) plane; in general, the result is a clump of data points. In order to fold information about these data to a one-dimensional space, Vokrouhlický et al. (2005) introduced a parametric relation

$$0.2\,H = \log\,(\Delta a/C)\ , \qquad (5)$$

between H and Δa. Here $\Delta a = a - a_{\rm c}$, where $a_{\rm c}$ basically shifts the origin in a near center of the family and C is a free parameter (both positive and negative). It is understood that the asteroids in the family do not satisfy a relation (5) for some particular $(a_{\rm c}, C)$ values. Rather, with fixing $a_{\rm c}$, or averaging results over some small interval of $a_{\rm c}$ values, the family is characterized by a distribution of C values. Thus we define a distribution function

$$\mathcal{D}(C) = \frac{dN}{dC}\ , \qquad (6)$$

where dN is the number of family asteroids in the (a, H)-strip generated by changing C in the range $(C, C+dC)$. Within this approach, the function $\mathcal{D}(C)$ contains entire information about the family. Any model that aims to reconstruct the family configuration in the (a, H) space could be validated/tested by matching the observed $\mathcal{D}(C)$ distribution. In what follows we use a pseudo-χ^2 method for this comparison.

The choice of the template function (5), and the related distribution (6) instead of the simple distribution $\mathcal{B}(a; H)$ of semimajor axis values, has been motivated by simple models involving purely either Yarkovsky dispersion or fragment ejection with velocity strictly inversely proportional to their size. Both would yield $\mathcal{D}(C)$ constant. So any deviations from a uniform $\mathcal{D}(C)$ distribution could be translated into deviations from these "toy models". Luckily, these go in a rather opposite way. A static model, with no dynamical evolution of the family, but velocity field either anisotropic and/or with a velocity dispersion for fragments of a given size, give typically $\mathcal{D}(C)$ concentrated near the origin or with a single maximum, asymmetric to the origin. Conversely, the model where combined Yarkovsky and YORP dynamical evolution of the family plays an important role results in $\mathcal{D}(C)$ that has two maximum values symmetrically offset from the origin $C = 0$.

3.2.2. Model

Figure 12 shows $\mathcal{D}(C)$ for the Eos family identified using the HCM cutoff velocity $V_{\rm c} = 55$ m/s (our nominal case).[12] In fact we show here directly the number $N_{\rm obs}(C)$ of Eos members in the interval $(C, C + \Delta C)$ values with $\Delta C = 4 \times 10^{-6}$ AU (there are 41 contributing bins/data points in this distribution), which is up to a scaling by ΔC identical to $\mathcal{D}(C)$. The result assumes $a_{\rm c}$ uniformly distributed in between 3.015 AU and 3.025 AU, very close to (221) Eos, and we always used asteroids with $a \le a_{\rm c}$ only. We decided to adopt this latter condition mainly because the region of the Eos family where $a > a_{\rm c}$ is influenced by the 9/4 mean motion resonance with Jupiter, as discussed in Sec. 3.1, and that might corrupt our analysis in an uncontrolled way. Nevertheless, the qualitative features discussed below are equally well identified in this twin part of the family. Most importantly, $\mathcal{D}(C)$ has a significant maximum at $C \simeq -7.5 \times 10^{-5}$ AU. The value $\mathcal{D}(0)$ represents only about one half of the maximum value at a very high statistical level (we use $\sqrt{N_{\rm obs}(C)}$ as quasi-errors of the values $N_{\rm obs}(C)$ in each of the bin in C). We also discarded from our analysis three objects, associated with the nominal Eos family, that have their $|C|$ value larger than 1.6×10^{-4} AU. In Fig. 3 we see them as "triangle" of bodies with $a \le 2.98$ AU and $H \le 12$ separated from the bulk of asteroid members. These are (1845) Helewalda, (8340) Mumma and (9711) Zeletava and we suspect these objects interlopers in the family (this is because within our scenario they are too far from the center of the family to be transported to their present location by Yarkovsky effect within a reasonable timespan). Indeed, in Sec. 3.4 we prove that the first two are spectrally alien to the Eos family members.

The maximum of $\mathcal{D}(C)$ misplaced from origin in Fig. 12 is due to the fact that in the (a, H) projection (see Fig. 3) small asteroids tend to preferentially populate regions at the outskirts of the family and leave its center underpopulated. Such a

[12] We have carefully checked, that up to a scaling factor due to a different total number of asteroids, very similar results are obtained for families with $V_{\rm c}$ in the range $50 - 60$ m/s.

distorted distribution of family members is hard to reconcile with any reasonable ejection field of fragments in the family-forming disruption event. In particular, it would mean two anti-aligned streams of fragments are thrown to preferentially populate extremal values of V_T. Such a geometry has never been observed in numerical simulations nor it would be expected by heuristic arguments. On the other hand, the Yarkovsky dispersal model offers a natural explanation for this feature.

In order to see the argument we need to briefly recall basic facts about the Yarkovsky-Öpik-Radzievskii-Paddack (YORP) effect (e.g. Rubincam, 2000; Vokrouhlický and Čapek, 2002; Bottke et al., 2003). YORP is only a different face of the same thermal phenomenon that causes Yarkovsky force to affect orbital motion, since YORP means thermal torque that affects rotation of irregularly-shaped bodies. The principal effect of YORP in our context is its ability to preferentially tilt obliquity toward extreme values (Čapek and Vokrouhlický, 2004) that, in turn, help the Yarkovsky forces to affect more the orbital semimajor axis (remind the diurnal variant of the Yarkovsky effect is likely to dominate for our bodies). With that conclusion, we would actually expect small family asteroids occupy extreme borders of the family in semimajor axis, leaving its center depleted after some time of evolution.

To test this hypothesis we constructed a simple numerical model with the goal to quantitatively match the observed distribution $\mathcal{D}(C)$. Its main features and parameters are as follows:

- We set initial distribution of fragments in the proper element space due to a finite (nonzero) velocity field from the parent-body disruption. To set things simple, we assume all velocity components, V_R, V_T and V_N along radial, transverse and normal directions as regards the parent body orbit, have the same Gaussian distribution with standard deviation $V_{\rm SD}$. We consider two models: (i) $V_{\rm SD} = V$ is a size-independent free parameter changed from zero to some maximum value of the order $\simeq 100$ m/s, or (ii) $V_{\rm SD} = V\,(5\,{\rm km}/D)$ is inversely proportional to the size D and V is again a free parameter of the model. The number of fragments used in our simulations is the same as number of observed asteroids in the family and we assign them the same value of absolute magnitude. This is converted to size D using the standard transformation with two different assumptions about the albedo value based on the observed Eos family data determined by Tedesco et al. (2002): (i) in a simpler approach we assign a value $p_V = 0.13$ to all asteroids in our model, since this corresponds to the mean value for Tedesco et al. Eos sample; (ii) in a more detailed approach, we assign random p_V to individual asteroids which obeys the observed distribution of p_V (Fig. 16). In the latter case, we run several simulations, since the size of each asteroid in this approach is not fixed but it is rather a statistical quantity. We then average over results of these several simulations.

- Apart from size and initial orbital elements (semimajor axis in particular), the asteroids are assigned some initial value of obliquity ϵ and angular velocity ω of rotation in our simulations. The initial orientation of spin axes is random in space, thus $\cos\epsilon$ is uniformly distributed in the interval $[-1, 1]$, while ω is assumed to have a Gaussian distribution peaked at 8 hr period (e.g. Binzel, 1988).

- Orbital evolution of each of the fragments is tracked individually. The semimajor axis a is assumed to undergo a steady change due to the Yarkovsky forces with a drift rate estimated by (e.g. Vokrouhlický, 1998, 1999)

$$\frac{da}{dt} = \kappa_1 \cos\epsilon + \kappa_2 \sin^2\epsilon \,, \qquad (7)$$

where κ_1 and κ_2 are functions depending on surface thermal parameters and the size. In accord with the numerical simulation above, we use the following set of thermal constants: thermal conductivity $K = 0.005$ W/m/K, specific heat capacity $C_p = 680$ J/kg/K, surface and bulk densities 1.5 and 2.5 g/cm^3. The Eq. (7) assumes (i) a spherical body residing on a circular orbit about the Sun, and (ii) a restricted, linearized analysis of the heat diffusion in the asteroid's surface. Nevertheless, we find it sufficient for the purpose of our work, because tests against complete numerical analysis show that Eq. (7) typically fails no more than by a factor 2.

- We also assume the two parameters of the rotation state, obliquity ϵ and rotation rate ω, undergo evolution due to the YORP effect. To model it we use

$$\frac{d\omega}{dt} = c_{\rm YORP}\, f(\epsilon)\,, \qquad (8)$$

$$\frac{d\epsilon}{dt} = c_{\rm YORP}\, \frac{g(\epsilon)}{\omega} \qquad (9)$$

(e.g. Vokrouhlický and Čapek, 2002; Čapek and Vokrouhlický, 2004). The f- and g-functions here are the median strength of the YORP torques derived by Čapek and Vokrouhlický (2004) for asteroids with a surface thermal conductivity $K = 0.005$ W/m/K. We also introduce a free parameter $c_{\rm YORP}$ by which we multiply $f-$ and $g-$functions in Eqs. (8) and (9), because we suppose modeling of the YORP effect is less certain than the Yarkovsky effect.

- Finally, our model contains a very simple implementation of the collisional dynamics; this is mainly because the Yarkovsky/YORP effects depend sensitively on the rotation state, which is itself dependent on collisions between asteroids. We neglect disruptive collisions, but include sub-critical collisions able to significantly re-orient spin axis of the body. An appropriate approach for this concept has been developed by Farinella et al. (1998) who obtained the following formula for the typical re-orientation timescale:

$$\tau_{\rm reor} = B\,(\omega/\omega_0)^{\beta_1} (D/D_0)^{\beta_2}\,, \qquad (10)$$

with $B = 84.5$ ky, $\beta_1 = 5/6$ and $\beta_2 = 4/3$, the reference size $D_0 = 2$ m and the rotation frequency ω_0 corresponding to the rotation period of 5 hr.

With a given initial configuration of the family, we run our code for a time T, ranging from 0.5 to 2 Gy, and we let the family evolve by the thermal effects. As mentioned above, apart from T we consider another two free-to-fit parameters: V and $c_{\rm YORP}$. To set a measure of a quantitative agreement between the simulation and the observed Eos family, we define a pseudo-χ^2 target function

$$\Psi_{\Delta C} = \sum_{\Delta C} \left(\frac{N(C) - N_{\rm obs}(C)}{N_{\rm obs}(C)} \right)^2\,, \qquad (11)$$

where formally the errors assigned to the number $N_{\rm obs}(C)$ in a given bin $(C, C + \Delta C)$ is $\sqrt{N_{\rm obs}(C)}$; $N(C)$ is the simulated number of asteroids in the appropriate C-bin. Our procedure seeks to minimize $\Psi_{\Delta C}(T, V, c_{\rm YORP})$ by variation of the three parameters in certain interval of values. Admissible solutions are characterized by $\Psi_{\Delta C}$ value of the order equal to the number of used bins in C (41 in our case), while solutions giving much larger $\Psi_{\Delta C}$ are incompatible with the observed family.

3.2.3. Results

For simplicity, we start with simulations where all asteroids were assumed to have a single albedo value $p_V = 0.13$. Figure 13 shows contour plots of $\Psi_{\Delta C}$ projected onto 2-D parameter planes T vs. $c_{\rm YORP}$, T vs. V and $c_{\rm YORP}$ vs. V. The best-fit solution for $N(C)$, together with the observed data $N_{\rm obs}(C)$ and their formal error-bars, is shown in Fig. 12. The results here hold for our simpler model, where V is size-independent, mean-quadratic velocity with which collisional ejecta are initially dispersed. Each time we picked the best $\Psi_{\Delta C}$-value along the suppressed dimension. The "critical" isoline value of 41 is plotted in bold; recall this value formally corresponds to solutions that barely match the observed family at the chosen 1σ-interval from all data points. If we adopted this threshold correct, the best solution we obtain for the three parameters is: $T = 1160^{+40}_{-100}$ My, $c_{\rm YORP} = 0.7^{+0.3}_{-0.2}$ and $V = 52^{+10}_{-14}$ m/s. Note, the three parameters are not uncorrelated in our solution, such that stronger YORP (i.e. larger $c_{\rm YORP}$) pushes the family age T to smaller values. The least correlated are $c_{\rm YORP}$ and V. The best-fit V of the velocity V is low and compatible with values expected from the hydrocode modeling. The initial family thus had about half extension in semimajor axis than the currently observed one. We also note that $c_{\rm YORP} \simeq 0$ value is strongly incompatible with the observations and thus YORP is needed for explaining observations. Its strength is, however, poorly constraint. The best-fit value of the target function (11) we found is $\Psi_{\Delta C} = 27.8$, smaller than 41, though we obviously admit a slight arbitrariness in our definition of formal standard deviation $\sqrt{N_{\rm obs}(C)}$ of number of objects in the C-strips (obviously any linear scaling in this quantity projects quadratically in the value of $\Psi_{\Delta C}$). Nevertheless, we consider

our fit is statistically significant.

Figures 14 and 15 show again the best fit solution for $N(C)$ and 2-D contour plots of the target function $\Psi_{\Delta C}$ in case of our refined model, when $V_{\rm SD} = V\,(5\,{\rm km}/D)$ (the mean-quadratic dispersal velocity is inversely proportional to size of fragments). Now V is a solved-for parameter fixing ejection velocity for $D = 5$ km fragments. Our best solution reads: $T = 1150^{+150}_{-100}$ My, $c_{\rm YORP} = 1.1^{+0.9}_{-0.7}$ and $V = 93^{+25}_{-20}$ m/s, where again the uncertainty limits are derived from the $\Psi_{\Delta C} = 41$ contour plot. The minimum target function value is $\Psi_{\Delta C} = 26.2$ below the admissible limit of 41, hence we consider the best solution statistically significant, and slightly better than in the previous solution. The general features of the solution are basically identical to the previous one with constant dispersal velocity $V_{\rm SD}$, confirming thus robustness of the solution. In our opinion, two results are the most interesting: (i) the estimated age of the Eos family consistently spans about the same interval of values, and (ii) the YORP strength within a factor $0.5-1$ corresponds to the modeled value by Čapek and Vokrouhlický (2004).

In the previous tests we used constant, and to-date, luminosity of the Sun. However, evolutionary models of the solar interior imply the Sun should have been about 25% fainter some 4 Gy ago (e.g. Bahcall et al., 2001; Table II). Smaller radiation flux in the past should produce weaker thermal effects, both the Yarkovsky force and YORP torque, and thus may modify our conclusions. For that reason we re-run our previous simulations taking into account variable solar luminosity. We approximate its time-dependence $L(t)$ with

$$L(t) \simeq L_0 \left[1 + 0.3\left(1 - \frac{t}{t_0}\right)\right]^{-1} , \qquad (12)$$

where L_0 is the current solar luminosity, $t_0 \simeq 4.57$ Gy is the age of the Sun and t is time (in Gy) measured from the origin of the Solar system (e.g. Bertotti et al., 2003; Chap. 7). Though not perfect, we find this approximation accurate enough for our tests. Our results indicate that while the best-fit values for $c_{\rm YORP}$ and V are comparable to our previous results the estimated age T of the family is little longer: $T = 1200^{+120}_{-100}$ My. Note, that according to our model Eq. (12) the mean solar luminosity over the past Gy was about 4% lower than today, and this nearly exactly projects into a $\simeq 4\%$ increase of the estimated Eos age. Thus for a moderately young family, such as Eos, the effect of fainter Sun in the past appears to be smaller than other uncertainties in our model. Perhaps a formal stretching of the age by the solar luminosity mean value is an acceptable approximation.

Finally, we test robustness of our solution on variation of the a priori unknown asteroid size (or, equivalently, their geometric albedo p_V value). To do so, we consider p_V distribution determined for 98 Eos members (selected from our nominal family at HCM $V_{\rm cut} = 55$ m/s) by Tedesco et al. (2002) – Fig. 16. We note the data show a considerable spread about the mean value of $p_V = 0.13$ used above, both to smaller and larger values. We run 10 simulations similar to those above using the mean ejection velocities of fragments inversely proportional to their D (our second model above), each time randomly assigning p_V to our asteroids to satisfy the observed distribution from Fig. 16. The best fit values of $\Psi_{\Delta C}$ ranged from 17 to 26, meaning thus our solutions each time fit reasonably well the Eos observed data (in fact, formally the best solutions). Considering the mean value of the best-fit solution for each of the free parameters (weighted by the best-fit value of the target function), and an envelope of the $\Psi_{\Delta C} = 41$ region in the parametric space, we obtain $T = 1300^{+150}_{-200}$ My, $c_{\rm YORP} = 0.7^{+1}_{-0.5}$ and $V = 70^{+20}_{-20}$ m/s. In comparison with the fixed albedo $p_V = 0.13$ model, we note only the estimate of the family age T changed a bit. This is because lower albedo values imply larger asteroid size and thus slower drift due to the Yarkovsky effect and strength of the YORP torques (note the p_V is somewhat skewed about the median toward smaller values).

3.3. Asteroids in the z_1 secular resonance

The importance of high-order secular resonances for the long-term fate of asteroid families has been studied only little so far. In part, this is because the topic is difficult from the orbital dynamics point of view, both as concerns analytical analysis and also as concerns numerical experiments that require tracking the asteroid motion over a long period of time. Milani and Knežević (1990, 1992, 1994) and Knežević and Milani (2003) have introduced and investigated these problems at some depth about a decade ago

only. These authors noticed that the Eos family is intercepted by the $z_1 = g+s-g_6-s_6$ resonance.[13] On a short-term (several My) no major effect on the family was expected, but Milani and Knežević (1990, 1992) posed a question about the long-term effects on the structure of the Eos family. This argument has been invoked several times afterword (e.g. Zappalà et al., 1990; Marzari et al., 1995) but without a deeper analysis.

The second reason why the high-order secular resonances received a little attention so far is that the asteroid families were assumed by many to deviate from simple models for other, more obvious reasons such as uncertain geometry of the initial velocity field. These were expected to mask any noticeable trace of the dynamics in weak secular resonances. This point of view has been, however, broken by Bottke et al.'s (2001) analysis of the Koronis family. These authors proved that the most significant, and also the most peculiar, feature of the Koronis family – the $\simeq 0.025$ proper eccentricity shift of all members in the Prometheus clan – derives from the interaction of the Yarkovsky-migrating orbits with the $g + 2g_5 - 3g_6$ secular resonance.

In what follows we aim to demonstrate that, albeit in a less spectacular way, the Eos family is clearly affected by the same process. As the asteroids migrate in the proper element space by the Yarkovsky effect, they get captured by the z_1 secular resonance and become driven to a specific region at the outskirts of the family as indicated in Fig. 4 and hinted from our numerical simulation described above.

3.3.1. Theoretical basis

A fundamental model of the perturbed asteroidal motion is the restricted three-body problem of Sun-Jupiter-asteroid (e.g. Morbidelli, 2002). Many aspects of asteroid motion, including fine perturbations, can be studied within this framework. Each of the various problems, such as motion in/near mean motion or secular resonances, is best understood if properly chosen variables are used. We thus start with a very brief recall of the variables tailored to the z_1 resonance.

The restricted three-body problem is a four degree of freedom autonomous system with the first three degrees describing three-dimensional motion of the test body (asteroid) and the last degree is Jupiter's longitude in orbit (removing time-dependence due to Jupiter's motion). In a Hamiltonian approach the asteroid-related degrees of freedom are standardly described with Delaunay variables $(L, G, H; l, g, h)$ or variables derived from them by canonical transformations (e.g. Morbidelli, 2002). For instance, it appears suitable for us to choose

$$\begin{pmatrix} L & l \\ G & g \\ H & h \end{pmatrix} \rightarrow \begin{pmatrix} \Lambda = L & \lambda = l+g+h \\ \Sigma = L-G & \sigma = -g-2h \\ \Theta = 2G-H-L & \theta = -h \end{pmatrix} , \tag{13}$$

where the new canonical variables $(\Lambda, \Sigma, \Theta; \lambda, \sigma, \theta)$ replace the original Delaunay set.

Representation of Jupiter's motion becomes more involved when secular variations of its orbital elements, mainly due to interaction with Saturn, are included in our analysis. This extends the problem by at least three degrees of freedom (e.g. Moons et al., 1998; Morbidelli, 2002); notably nonsingular elements $(e'\cos\varpi', e'\sin\varpi'; \sin(I'/2)\cos\Omega', \sin(I'/2)\sin\Omega')$ of Jupiter are going to be expressed as harmonic functions of the secular angles $\lambda_5 = g_5 t$, $\lambda_6 = g_6 t$ and $\lambda_{16} = s_6 t$ (here g_5, g_6 and g_{16} are the corresponding fundamental frequencies of the planetary system; e.g. Morbidelli, 2002). The conjugated momenta to these angular variables are Λ_5, Λ_6 and Λ_{16}. Using another canonical transformation

$$\begin{pmatrix} \Sigma & \sigma \\ \Lambda_6 & \lambda_6 \\ \Lambda_{16} & \lambda_{16} \\ \cdots & \cdots \end{pmatrix} \rightarrow \begin{pmatrix} -\Sigma & -\sigma-\lambda_6-\lambda_{16} \\ \Sigma-\Lambda_6 & -\lambda_6-\lambda_{16} \\ \Lambda_6-\Lambda_{16} & -\lambda_{16} \\ \cdots & \cdots \end{pmatrix} , \tag{14}$$

we obtain variables suitable to analysis of motion in the z_1 resonance, because $\Sigma' = -\Sigma$ and $\sigma' = -\sigma-\lambda_6-\lambda_{16}$ appear to be resonant momentum and critical argument of this secular resonance. In a simplified model where all other degrees of freedom are eliminated by averaging, the resonance becomes represented by a one-dimensional model

[13] This resonance causes the secular angle to $\varpi + \Omega - \varpi_6 - \Omega_6$ librate, rather than circulate, on a typical timescale of $3-5$ My; here ϖ is longitude of pericenter and Ω is longitude of node of the asteroid, while ϖ_6 and Ω_6 are the same parameters for Jupiter. In an analytical theory, such as Milani and Knežević (1990, 1992), the $g+s-g_6-s_6$ frequency appears as a small divisor associated with this resonance.

in resonant variables (Σ', σ'). In particular, outside the resonance σ' circulates with secular frequency $-\dot{\sigma} - g_6 - s_6$ (overdot is a time derivative), while inside the resonance, i.e. near the hypersurface $\mathcal{Z}_1 : -\dot{\sigma} - g_6 - s_6 \simeq 0$, σ' librates. Since $\Sigma' = \sqrt{a}\,(1 - \sqrt{1-e^2})$, and a is constant due to eliminated λ, the resonance produces a long-term variations in eccentricity e of the orbit. Because Θ is also constant, due to the elimination of θ, we have a quasi-integral $\sqrt{a(1-e^2)}\,(2 - \cos I)$. Thus the long-term variations of orbital eccentricity e and inclination I are resonantly coupled and the inclination has also long-term variations.

Additional difficulty arises when a non-gravitational force, like the Yarkovsky effect, is included in the model. In the simplest representation we could retain only the major secular effect, namely a steady change of the semimajor axis a. Because the characteristic timescale for this perturbation is very long, even if compared to the secular dynamics in the weak z_1 resonance, one might still assume a constant during one resonant cycle of σ' and investigate evolution of the system under slowly (adiabatically) changing parameter a. This approach could, in principle, yield capture probabilities in the z_1 resonance for bodies with different rate of change in a. Once in the resonance, one would assume the orbits shows coupled oscillations in e and I over-imposed over a slow migration along $\mathcal{Z}_1$ hypersurface until conditions to leave the resonance are satisfied. However, it is not our goal to present that detailed analysis and we mainly rely on results of numerical experiments.

3.3.2. z_1 resonance in the Eos family

We first analyze residence of the Eos asteroids inside the z_1-resonance. We consider the family identified using HCM and $V_c = 55$ m/s; in Sec. 2 we found it contains some 4394 members. We numerically integrated orbits of these asteroids for 10 My and computed behavior of the critical angle σ' defined above. For that purpose we use the same symplectic integrator as described above, but we do not include the Yarkovsky forces at this stage keeping just gravitational perturbations from giant planets. As above, the planetary initial data are from `JPL DE405` ephemerides and the asteroid initial data from the `AstOrb` database. To simplify our procedure, we first output mean orbital elements for each of the asteroids every 1.5 ky using Fourier filtering of high-frequencies from the osculating orbital elements. The mean orbital elements are then processed with the aim to identify asteroids residing in the z_1 resonance. In particular, we use running window filter about 750 ky wide and with steps of 100 ky. On each of these intervals we Fourier analyze the time series of the non-singular orbital elements and we determine frequency and phase of the proper and forced terms. Among the forced terms we are principally interested to isolate the g_6 and s_6 frequencies and their associated phases. The phases are used to construct the critical angle σ' of the resonance, where ϖ and Ω are substituted by the phases of the corresponding proper terms in non-singular orbital elements, and ϖ_6 and Ω_6 are the phases of the corresponding forced terms. We replace the momentum Σ' with the frequency combination $g + s - g_6 - s_6$ and plot asteroid tracks in the configuration space of these two variables. Figure 17 shows several examples including asteroid (221) Eos that is trapped in the z_1 resonance (e.g. Milani and Knežević, 1990, 1992). We show both motion of asteroids whose σ' librates at small amplitude, thus residing near the center of the resonance, the case for which σ' alternates between libration and circulation, thus residing near the separatrix of the resonance, and the case for which σ' circulates. Typical libration periods of σ' inside the resonance are between $3 - 5$ My and the resonance width is about 0.8 arcsec/yr. Figure 4 then helps to translate this information into which portion of the proper element space this resonance occupies. Interestingly, we note the z_1 resonance stretches over a fairly non-negligible fraction of the Eos family. We find that 13% (575 out of 4394) Eos family members are captured inside this resonance.[14] Figure 18 shows the distribution of the critical angle σ' of all 4394 asteroids associated with the family (solid line). Unlike the previous studies, Brouwer (1951) or Milani and Knežević (1992), we show σ' distribution is uniform up to random fluctuations. For sake of completeness we also show σ' histogram constructed from 58 asteroids known as Eos members to Brouwer (1951), truly indicating some degree of non-uniformity.

[14] We have also analyzed residence of Eos members in the $g + s - g_5 - s_7$ secular resonance and found only $\simeq 1.5\%$ of them librate. This is because this resonance is much weaker (e.g. Milani and Knežević, 1990, 1992).

The reason though is that large asteroids near (221) Eos are preferentially located inside the z_1 resonance and thus have σ' values confined near the value of stable point of this resonance producing thus the observed effect (the same applies to a lesser degree to data reported by Milani and Knežević, 1992). Hence the previously reported non-uniform distribution of σ' is a selection effect unrelated to the age of the family.

On a short term, such as the 10 My integration we performed, no instability can be observed and it is also quite possible that without the dissipative perturbing effects the z_1 resonance would not produce any significant disorder in the Eos family. Nevertheless, as shown in Fig. 19, it produces a non-negligible spread of the family in eccentricity and inclination, contributing thus to the old problem with this family (see Sec. 1). This is partly surprising given the weakness of the resonance: for a near-separatrix case, such as (2216) Kerch, the the synthetic proper eccentricity, determined from an integration spanning $\simeq 1$ My, may oscillate in time by nearly 0.02. This is about a half of the total eccentricity extension of the family, thus a significant fraction. The same applies to the inclination. The results shown in Fig. 19 were obtained by considering orbital evolution over 700 ky windows, sliding in 100 ky steps, from our 10 My integration. In each of the windows we Fourier decomposed non-singular orbital elements related to both eccentricity and inclination and eliminated the planetary, forced terms. With that procedure we identified the proper terms and we determined proper eccentricity and proper sine of inclination as amplitudes of these terms (see Knežević and Milani, 2000).

The role of the z_1, however, changes –and strengthens– when the Yarkovsky forces are taken into account. As demonstrated by our numerical integration above (see also Vokrouhlický and Brož, 2002), migrating asteroids due to the Yarkovsky effect may encounter the z_1 resonance and become long-term captured before being ejected again. The captures may last several tens to several hundreds of My. During the capture period, the orbit is confined inside the z_1 resonance but the Yarkovsky forces keep changing the value of semimajor axis. As a result, orbits follow the resonance, moving along it like on a "slide". Asteroids drifting toward smaller value of the semimajor axis, in particular, are forced to decrease their mean value of the inclination and eccentricity when confined to the resonance. In Sec. 2 we suggested this mechanism may populate the anomalous tail of the Eos family and we have seen a direct confirmation of this process in our simulation of the synthetic family. We thus selected Eos family asteroids whose proper elements satisfy $a \leq 3.01$ AU, $e \leq 0.065$ and $\sin I \leq 0.17$, and we checked their residence in the z_1 resonance. Not surprisingly, we found 67% (246 out of 366) of these orbits reside in this resonance. This much higher fraction, as compared to the whole Eos family as a whole, suggests asteroids has been transported to this outskirt place via confinement in the z_1 resonance combined with the Yarkovsky-induced drift.

3.4. Additional data and observations

In order to substantiate our previous interpretations and conclusions, based uniquely on a dynamical HCM identification of the family in the proper element space, we conducted spectroscopic observations of about a dozen asteroids in the Eos zone. Our objective was to support relation of particular asteroids to the family in some cases or reject their relation to the family in some other cases.

In the first case, we focused on asteroids located inside the z_1 secular resonance and having anomalously small value of proper eccentricity and inclination as compared to the other Eos members (Sec. 3.3). Finding them spectrally compatible with Eos asteroids would support our scenario of transporting objects to this outskirt zone in the proper element space. In a less spectacular way, this bears similarity to Zappalà et al. (2000) spectral identification of Eos fugitives inside the 9/4 MMR.

In the second case, we focus on suspected interlopers in the Eos family. Those are suggested by our model to fit the Eos family in the proper semimajor axis a vs. absolute magnitude H projection (Sec. 3.2). Notably, objects with anomalously large value of the C parameter from Eq. (5), or in other words disconnected from the bulk of family objects in the (a, H) plane (Fig. 3), cannot fit our Yarkovsky-transport scenario being too offset from the family center for their large size. Within our model, we demand them being aliens

in the family and spectroscopic information may offer a confirmation. Note, in fact, that we have discarded three of such asteroids from our fitting procedure in Sec. 3.2 under this assumption.

We start with our own observations in Sec. 3.5, and to strengthen our conclusions we also make use of the most updated SDSS database in Sec. 3.6 (performing thus a more detailed look at the Eos family than Nesvorný et al., 2005a).

3.5. Spectroscopy

3.5.1. Asteroids inside the z_1 resonance

Table 3 summarizes our target asteroids and the observational circumstances. The asteroids inside the z_1 stream are generally very small, so their spectroscopy is challenging even with moderately large instruments. Our sample of the observed asteroids is random, mainly deriving from observational possibilities, from the used instruments and from the available observation timespan. The Kitt Peak National Observatory (KPNO) and Palomar observations reported in this and the following sections were acquired both through a dedicated program for this work and also as targets of opportunity during the ongoing Small Main-Belt Asteroid Spectroscopic Survey (SMASS). The KPNO observations used the RCSP spectrometer on the Mayall 4-m telescope, generally covering the spectral range $500 - 920$ nm, and the Palomar observations used the Double Spectrograph on the Hale 5-m telescope and generally covered the spectral range $320 - 950$ nm. Details of the observations and reductions can be found in Binzel et al. (2004), which used the same telescopes and instruments and had identical data reduction and analysis techniques. To summarize, well-known solar-type stars were observed frequently during the night interspersed with target objects in order to account for the influence of the solar spectrum and the terrestrial atmosphere on the target asteroids. Commonly used IRAF routines and packages were used to extract the spectra of the asteroids and stars, and a set of mean extinction coefficients appropriate for each observing site was used for additional corrections. The resulting asteroid/star ratios were then tied into the spectral taxonomy of Bus and Binzel (2002a,b).

Figure 20 shows the collected reflectance spectra for our 4 objects, indicating three are of T-class and one –(62948) 2000 VE32– is of X-type. As discussed in Sec. 2.2, the T-types are well compatible with Eos family and we thus interpret these three objects as Eos members that has been likely closer to the center of the family in the past but were pushed to their present locations by the Yarkovsky forces. The X-type asteroid in the same zone appears to be an interloper object equally caught in the z_1 resonance. The $\sim 25\%$ fraction of alien asteroids in our observing sample, though certainly not much statistically significant, might correspond to the overall $\sim 25 - 30\%$ interloper fraction inside the Eos family inferred from spectroscopic observation of large members (see Sec. 2.2).

3.5.2. Suspected interlopers

Next we comment on observations of suspected interlopers in the Eos family (Table 4). In this case we used three sites and instruments to collect the data: (i) the 1.52-m European Southern Observatory (ESO) telescope at La Silla, (ii) 4-m telescope at KPNO, and (iii) 5-m telescope at Palomar.

The observations carried out at La Silla were an extention of the S^3OS^2 survey (Lazzaro et al., 2004) during two observational runs in March and November 2002. The ESO 1.52-m telescope was equipped with a Boller and Chivens spectrograph and a 2048×2048 pixels CCD detector with a readout noise of $7[e^-$ rms] and square pixels of $15\,\mu$m. A grating of 225 gr/mm with a dispersion of 33 nm/mm in the first order was used. This configuration resulted in an useful spectral range of $490 - 920$ nm with a FWHM of 1 nm. The spectra were taken through a 5 arcsec slit oriented in the East-West direction. The spectral data reduction was performed using the IRAF package and the classical procedure with averaged bias and dome flat-fields. Wavelength calibration was performed using a He-Ar lamp, which spectrum was obtained several times during each night. The spectra were corrected for airmass by using the mean extinction curve of La Silla (Tüg, 1977). Different solar analogs (Hardorp, 1978) were observed in each observational run in order to compute reflectivities. Tests made using different solar analogs produced differences in the reflectance spectra smaller than 1%/100 nm. The solar analogs HD44594 and HD20630 were used in the March and November

run, respectively. The obtained asteroid spectra have been normalized around 550 nm by convention.

Figure 21 folds all acquired spectra into a common frame with a necessary shift in the reflectance scale for visibility. The lowest shown are three X-type objects, certainly spectrally alien to the Eos family. The same holds for (251) Sophia, a large target seemingly offset in semimajor axis from the family members of comparable sizes (Fig. 22). Our data make us classify this target as L-type, dissimilar to the main KTD sequence in the family. All these four objects are our searched, high-C interlopers. Further objects require closer discussion.

Asteroid (8340) Mumma is the only object we observed with semimajor axis smaller than $a_{\rm c} = 3.02$ AU and a high value of the C parameter (see Fig. 22 where we summarize positions of our observed targets in the (a, H) projection; an X-type asteroid (1845) Helewalda was added here for sake of interest, Monthé-Diniz et al., 2005). We note, that this object is also located inside the z_1 secular resonance, being its by far largest body. With its semimajor axis $a = 2.97$ AU it is largely offset from the family center, so that the Yarkovsky forces could not have transported it to its location from near the family center in $\simeq 1$ Gy, i.e. the age of family estimated in Sec. 3.2. From that perspective we require it interloper. We find (8340) Mumma a possibly D-type object, whose spectrum steepness is however anomalous even within this class (Fig. 21) and also within other D-type asteroids embedded inside the Eos family. This hints about its incompatibility with the family. In the next section we find using SDSS data highly likely that (8340) Mumma is indeed an interloper in the family.

Asteroid (27789) 1993 BB7 has a spectrum resembling that of the K-type asteroids, suggesting its membership in the family. We find this link possible in spite its rather large value of $C = 1.77 \times 10^{-4}$ AU. Figure 22 suggests this object resides right at the possible limit of the family, whose offset in semimajor axis (thus in C) might have been increased by a favorable initial position and/or jumping through the 9/4 MMR on its way toward larger semimajor axis values. Indeed, the finite width of this resonance, $0.005 - 0.01$ AU (Figs. 7 and 8), help dispersing the family more on the right hand side of the 9/4 MMR.

Out of the two Xk-type classified objects – (11993) 1999 XX and (36151) 1999 RG193 – the first lies again close enough to the family edge that it might be compatible as a family member even in our scenario. However, given their flat spectra we consider them rather alien to the family. The most intrigue case is that of (1755) Lorbach, a T-type asteroid well beyond a reasonable association with the family (Fig. 22; note also this asteroid becomes associated with the Eos family only at the HCM velocity $V_{\rm c} = 58$ m/s so formally it is not a member of our nominal Eos family). Since T-types are not exclusively members in the Eos family but are in a small number found through the whole main asteroid belt we find plausible that (1755) Lorbach is an interloper in the Eos family. We made a search in the two most wealthy spectroscopic databases – SMASS and S^3OS^2 – and found there are 49 T-type asteroids classified. Out of these, only 5 are clear members of the Eos family.[15] The surrounding zone of the Eos family holds another 12 T-type asteroids in the SMASS and S^3OS^2 catalogues that are certainly not related to this family.[16] Interestingly, many of them have semimajor axes values in a tight zone between 3.12 AU and 3.19 AU. This observation suggests the background zone near the Eos family contains a non-negligible number of T-type asteroids, of which (1755) Lorbach may be a member. In the next section, we use SDSS data to bring another piece of evidence for this asteroid being alien to the Eos family.

3.6. SDSS data

Additionally to the narrow-band spectroscopy, we also used a large database of the SDSS five broad-band photometry to characterize reflectance of smaller asteroids inside the Eos family. We use the same methodology and data analysis as in Nesvorný et al. (2005a), though we make advantage of the third, updated release of the SDSS data. This source contains five color information

[15] There are 22 more T-type Eos members found through observing programs dedicated to this family (Doressoundiram et al., 1998; Monthé-Diniz et al., 2005), but we consider better to base our argument here on the mentioned all-belt programmes.

[16] These are: (96) Aegle, (465) Alekto, (596) Scheila, (717) Wisibada, (979) Ilsewa, (986) Amelia, (987) Wallia, (1006) Lagrangea, (1209) Pumma, (1306) Scythia, (2813) Zappala, (2929) Harris.

about 43424 individual moving objects that were positively identified with known sources. Searching in this database, we found 985 Eos members. We constructed normalized reflectance spectra and computed their principal components PC_1 and PC_2 (see Eq. (1) in Nesvorný et al., 2005a). For the final analysis we choose only 499 asteroids with formal PC_1 and PC_2 errors smaller than 0.1.

Figure 23 shows our results. Left panel gives the mean 5-point spectrum (dashed line) together with a formal standard deviation strip (shaded zone). The overall shape of the mean spectrum well matches T-type classification, however this comparison might be partially flawed with properties of the SDSS broad-band filters. Namely, the long-wavelength SDSS z filter spans a rather broad wavelength interval centered about 909.7 nm (e.g. Fukugita et al., 1996) and it effectively smears to some degree the absorption feature near $0.9\,\mu$m crucial for the spectral taxonomy in optical. Thus a more quantitative results may be achieved using analysis of the family projected onto the principal component axes – right panel in Fig. 23. Though a large scatter of data-points is noticeable here, likely corresponding to the variation of the spectral classes concluded from narrow-band spectroscopy data, the Eos members do constitute a distinct cluster in these variables (such as they have been identified through clustering analysis in the proper element space). Assuming the Eos cluster represents a formal relation of the two principal component parameters PC_1 and PC_2, we may determine confidence levels corresponding to this relationship (see e.g. Bertotti et al., 2003, Sec. 20.5). In Fig. 23 we specifically show the ellipses of the 90% and 99% Eos membership based of this analysis. Asteroids close to these limits, or beyond them, happen to be weakly connected with the bulk of the family and likely represent outlier bodies. We searched large objects beyond, or close to, the 90% confidence level which correspond to a large $|C|$ constant from Eq. (5), i.e. which are detached from the family in the plane of proper semimajor axis and absolute magnitude. We found four cases of interest (shown as crosses in Fig. 23). Asteroids (4843) Megantic and (4431) Holeungholee, denoted 3 and 4, have been both classified X-types using narrow-band spectroscopy (Lazzaro et al., 2004; Monthé-Diniz et al., 2005). Indeed, they are shifted out of the center of Eos group toward smaller value of PC_1 component indicating their flatter spectrum. The amount of the shift places them at the outskirt of the family and we thus confirm conclusions from the narrow-band spectroscopy analysis that these two objects are very likely interlopers in the Eos family. The other two cases are (8340) Mumma, denoted 1, and (1755) Lorbach, denoted 2. These are particularly interesting, because the analysis of the narrow-band photometry reported in Sec. 3.5 let them classified D and T. These classes are generally compatible with the family (Sec. 2.2), but this does not mean that an interloper asteroid might not accidentally belong to the D or even T taxonomy class. In the (8340) Mumma case, we indeed observe that the SDSS photometry places it toward the D group (high PC_2 value). In fact its displacement in PC_2 component, relative to the family center, is larger than for other D-type Eos members, so that (8340) Mumma occurs beyond the 99% confidence level of the family PC_1-PC_2 identification. Thus the SDSS data suggest that (8340) Mumma appears to be alien in the Eos family, in spite its D taxonomic classification. The same analysis results in merely rejecting (1755) Lorbach as an Eos member in spits its T taxonomic classification since this asteroid resides at the 90% confidence level line for being associated with the Eos family using the clustering in (PC_1, PC_2) plane.

Finding these last two asteroids incompatible with membership to the Eos family is "good news" since their respective values of the C parameter are $C = -2.1 \times 10^{-4}$ AU for (8340) Mumma and $C = 5.1 \times 10^{-4}$ AU for (1755) Lorbach, far too large to explain them using the Yarkovsky diffusion model (see e.g. Figs. 12, 14 and 22).

4. Conclusions

This work represents a progress in understanding the structure and history of the Eos asteroid family. In particular, with the Yarkovsky diffusion model we were able to match several outstanding features seen in the proper element space such as the sharp termination at the 7/3 MMR and formation of an asteroid stream adhered to the z_1 secular resonance.[17] Our model also stands the

[17] Here we also recall the work of Tsiganis et al. (2003) who used the same model as here to satisfactorily interpret the

test of comparing population of the Eos members of both sides of the 9/4 MMR by correctly predicting their relative fraction, and it provides the only platform to understand the concentration of small asteroids toward the extreme values of the semimajor axis inside the family (see also Vokrouhlický et al., 2005). An important circumstance of this matching the semimajor axis distribution of small members is our ability to constrain the age T of the Eos family. Our estimate, $T = 1.3$ Gy some 30% younger than used by Nesvorný et al. (2005a), actually brings the Eos "data-point" closer to the empirical relation between the average spectral slope PC_1 within the family and its age determined by these authors (see Fig. 11 in Nesvorný et al., 2005a).

The still puzzling status of the Eos parent-body mineralogy, reflected as a taxonomic non-uniform taxonomiy of nearly-certain members of this family, makes us to not overvalue our spectral analyses and inferences from them in Sec. 3.4. Nevertheless we find satisfactory that majority of randomly chosen small asteroids inside the z_1 stream from the Eos family are spectrally compatible with its members. Similarly, we showed that many of asteroids that would appear puzzling within our Yarkovsky-diffusion scenario (those having large C parameter), have flat spectra what is in conflict with Eos membership. In the case of asteroids (8340) Mumma and (1755) Lorbach, additional analysis of the SDSS 5-color photometry helped us to argue in favor of their mismatch with the family.

At the same time, we do admit our work does not fully resolve the old-standing problem of large eccentricity and, especially, inclination dispersion of the Eos family (Sec. 1). In our view this problem has most likely to do with a combination of two effects. First, Bottke et al. (1994) analysed statistical properties of relative velocity for main belt projectiles on a putative Eos family progenitor (assumed for simplicity to have the same orbit as Eos). They found the relative velocity component normal to the Eos plane is by a factor $\simeq 4$ larger than the along-track relative velocity component, while the radial relative velocity component is somewhat intermediate. Numerical modelling work of large asteroid disruptions shows that the ejecta velocity field is always anisotropic. More interesting for us, this anisotropy often (especially for impacts with nonzero inclination) bear imprints of the relative velocity of the projectile such that the fastest released fragments fly approximately along the direction given by the relative projectile velocity (or within some cone around it). Recalling, from Gauss equations, that the initial semimajor axis dispersion derives from the along-track velocities of ejecta, while the inclination dispersion derives from the normal velocities of ejecta (for the eccentricity we have a combination of the along-track and radial velocities of ejecta), we naturally expect larger initial dispersion of the family in the inclination and eccentricity.

To make the comparison quantitative, we note that our best solution from Sec. 3.2 indicates that $D \simeq 4$ km asteroids, dominantly populating the family, were ejected with the typical along-track velocity component of $\simeq 100$ m/s (we investigated only the semimajor axis dispersion). If this value is used also for the other two components, radial and normal, we would expect maximum eccentricity and inclination initial dispersions of $\simeq 0.024$ and $\simeq 0.012$. The observed dispersion is $\simeq 0.040$ and $\simeq 0.025$, larger than the maximum estimated values. Here, however, we believe one should account for the larger characteristic velocities of ejecta in the normal and radial directions as explained above. This effect, in combination with the z_1 resonance perturbations, should easily explain the apparent mismatch of the expected (from along-track velocities) and observed dispersion of the Eos family in e and I.[18]

After Koronis (Bottke et al., 2001), Eos is the second asteroid family which here received a thorough analysis using the modern view of initial cluster from parent fragmentation evolving both via collisional and dynamical effects. More studies about other families will be useful, in particular to constrain their ages, a vital information to trace overall history of the main belt of asteroids.

resonant population of asteroids inside the 7/3 MMR.

[18] The same feature is seen in the young Veritas family (e.g. Nesvorný et al., 2003), whose initial velocity field holds a high degree of anisotropy. For instance, from the relative measure of the inclination and semimajor axis dispersion of Veritas multi-kilometer members we determine that the ratio of the mean normal vs transverse velocity components was $3 - 5$ in this case. It is tempting to assume a similar explanation as for the Eos.

This work, DV and MB, has been supported by the Grant Agency of the Czech Republic, grant 205/05/2737. The work of DL has been supported by CNPq through grant No. 306605/2003-1. We thank Andrea Milani and Zoran Knežević for providing us with their numerically computed secular proper frequencies across the whole asteroid belt and a related software allowing to display location of various high-order secular resonances. We also thank Hal Levison for the suggestion to study the role of faint young Sun (Sec. 3.2) and Zeljko Ivezić for providing us with the SDSS moving objects catalogue (Data release 3.0). Observations obtained at the Hale Telescope, Palomar Observatory are part of a collaboration between the California Institute of Technology, NASA/JPL, and Cornell University.

REFERENCES

Bahcall, J.N., Pinsonneault, M.H., Basu, S., 2001. Solar models: Current epoch and time dependences, neutrinos, and helioseismological properties. Astrophys. J. 555, 990–1012.

Bell, J.F., 1989. Mineralogical clues to the origin of asteroid dynamical families. Icarus 78, 426–440.

Bell, J.F., Hawke, B.R., Owensby, P.D., 1987. Carbonaceous chondrites from S-type asteroids? Bull. Am. Astron. Soc. 19, 841.

Bendjoya, P., Zappalà, V., 2002. Asteroid family identification. in: *Asteroids III* (W.F. Bottke, A. Cellino. P. Paolicchi and R.P. Binzel, Eds.), pp. 613–618. Arizona University Press, Tucson.

Benz, W., Asphaug, E., 1999. Catastrophic disruptions revisited. Icarus 142, 5–20.

Bertotti, B., Farinella, P., Vokrouhlický, D., 2003. *Physics of the Solar System*. Kluwer Academic Publishers, Dordrecht.

Binzel, R.P., 1988. Collisional evolution in the Eos and Koronis asteroid families: Observational and numerical results. Icarus 73, 303–313.

Binzel, R.P., Rivkin, A.S., Stuart, J.S., Harris, A.W., Bus, S.J., Burbine, T.H., 2004. Observed spectral properties of near-Earth objects: results for population distribution, source regions, and space weathering processes. Icarus 170, 259–294.

Bottke, W.F., Nolan, M.C., Greenberg, R., Kolvoord, R.A., 1994. Velocity distributions among colliding asteroids. Icarus 107, 255–268.

Bottke, W.F., Vokrouhlický, D., Brož, M., Nesvorný, D., Morbidelli, A., 2001. Dynamical spreading of asteroid families via the Yarkovsky effect: The Koronis family and beyond. Science 294, 1693–1695.

Bottke, W.F., Vokrouhlický, D., Rubincam, D.P., Brož, M., 2003. Dynamical evolution of asteroids and meteoroids using the Yarkovsky effect. in: *Asteroids III* (W.F. Bottke, A. Cellino. P. Paolicchi and R.P. Binzel, Eds.), pp. 395–408. Arizona University Press, Tucson.

Bottke, W.F., Durda, D.D., Nesvorný, D., Jedicke, R., Morbidelli, A., Vokrouhlický, D., Levison, H.F., 2005a. The fossilized size distribution of the main asteroid belt. Icarus 175, 111–140.

Bottke, W.F., Durda, D.D., Nesvorný, D., Jedicke, R., Morbidelli, A., Vokrouhlický, D., Levison, H.F., 2005b. The collisional evolution and dynamical depletion of the main belt: Constraints on the initial population and formation time of Jupiter. Icarus, in press.

Brouwer, D., 1951. Secular variations of the orbital elements of minor planets. Astron. J. 56, 9–32.

Brown, E.W., 1932. Observation and gravitational theory in the Solar System. Publ. Astron. Soc. Pacific 44, 21–40.

Bus, S.J., Binzel, R.P., 2002a. Phase II of the small main-belt asteroid spectroscopic survey. The observations. Icarus 158, 106–145.

Bus, S.J., Binzel, R.P., 2002b. Phase II of the small main-belt asteroid spectroscopic survey. A feature-based taxonomy. Icarus 158, 146–177.

Campo Bagatin, A., Petit, J.-M., 2001. Effects of the geometric constraints on the size distributions of debris in asteroidal fragmentation. Icarus 149, 210–221.

Carpino, M., Gonczi, R., Farinella, P., Froeschlé, Ch., Froeschlé, C., Paolicchi, P., Zappalà, V., 1986. The accuracy of proper orbital elements and the properties of asteroid families: Comparison with the linear theory. Icarus 68, 55–76.

Čapek, D., Vokrouhlický, D., 2004. The YORP effect with finite thermal conductivity. Icarus, in press.

Carruba, V., Burns, J.A., Bottke, W.F., Nesvorný, D., 2003. Orbital evolution of the Gefion and Adeona asteroid families: close encounters with massive asteroids and the Yarkovsky effect. Icarus 162, 308–327.

Cellino, A., Bus, S.J., Doressoundiram, A., Lazzaro, D., 2002. Spectroscopic properties of asteroid families. in: *Asteroids III* (W.F. Bottke, A. Cellino. P. Paolicchi and R.P. Binzel, Eds.), pp. 633–643. Arizona University Press, Tucson.

Cellino, A., Michel, P., Tanga, P., Zappalà, V., Paolicchi, P., Dell'Oro, A., 1999. The velocity-size relationship for members of asteroid families and implications for the physics of catastrophic collisions. Icarus 141, 79–95.

Clark, B.E., Bell, J.F., Fanale, F.P., O'Connor, D.J., 1995. Results of seven-color asteroid survey: Infrared spectral observations of ≈50-km size S-, K-, and M-type asteroids. Icarus 113, 387–402.

Davis, D.R., Farinella, P., Paolicchi, P., Weidenschilling, S.J., Binzel, R.P., 1989. Asteroid collisional history: Effects on sizes and spins. in: *Asteroids II* (R.P. Binzel, T. Gehrels and M.S. Matthews, Eds.), pp. 805–826. Arizona University Press, Tucson.

Dell'Oro, A., Bigongiari, G., Paolicchi, P., Cellino, A., 2004. Asteroid families: evidence of ageing of the proper elements. Icarus 169, 341–356.

Dermott, S.F., Grogan, K., Durda, D.D., Jayaraman, S., Kehoe, T.J.J., Kortenkamp, S.J., Wyatt, M.C., 2001, Orbital evolution of interplanetary dust. in: *Interplanetary Dust* (E. Grün, B.A.S. Gustafson, S.F. Dermott and H. Fechtig, Eds.), pp. 569–639. Springer, Berlin.

Dohnanyi, J.W., 1969. Collisional models of asteroids and their debris. J. Geophys. Res. 74, 2531–2554.

Doressoundiram, A., Barucci, M.A., Fulchignoni, M., Florczak, M., 1998. Eos family: A spectroscopic study. Icarus 131, 15–31.

Farinella, P., Vokrouhlický, D., 1999. Semimajor axis mobility of asteroidal fragments. Science 283, 1507–1510.

Farinella, P., Vokrouhlický, D., Hartmann, W.K., 1998. Meteorite delivery via Yarkovsky orbital drift. Icarus 132, 378–387.

Farinella, P., Carpino, M., Froeschlé, Ch., Froeschlé, C., Gonczi, R., Knežević, Z., Zappalà, V., 1989. The ages of asteroid families. Astron. Astrophys. 217, 298–306.

Fujiwara, A., 1982. Complete fragmentation of the parent bodies of Themis, Eos, and Koronis families. Icarus 52, 434–443.

Fukugita, M., Ichikawa, T., Gunn, J.E., Doi, M., Shimasaku, K., Schneider, D.P., 1996. The Sloan Digital Sky Survey photometric system. Astron. J. 111, 1748–1756.

Hardorp, J., 1978. The Sun among the stars. Astron. Astrophys. 63, 383–390.

Hirayama, K., 1918. Groups of asteroids probably of common origin. Astron. J. 31, 185–188.

Ivezić, Z., and 32 collaborators. Solar system objects observed in the Sloan Digital Sky Survey commissioning data. Astron. J. 122, 2749–2784.

Ivezić, Z., Lupton, R.H., Jurić, M., Tabachnik, S., Quinn, T., Gunn, J.E., Knapp, G.R., Rockosi, C.M., Brinkmann, J., 2002. Color confirmation of asteroid families. Astron. J. 124, 2943–2948.

Jedicke, R., Nesvorný, D., Whiteley, R., Ivezić, Z., Jurić, M., 2004. An age-colour relationship for main-belt S-complex asteroids. Nature 429, 275–277.

Jurić, M., and 12 collaborators, 2002. Comparison of positions and magnitudes of asteroids observed in the Sloan Digital Sky Survey with those predicted for known asteroids. Astron. J. 124, 1776–1787.

Knežević, Z., Milani, A., 2000. Synthetic proper elements for outer main belt asteroids. Celest. Mech. Dyn. Astron. 78, 17–46.

Knežević, Z., Milani, A., 2003. Proper element catalogs and asteroid families. Astron. Astrophys. 403, 1165–1173.

Lazzaro, D., Angelia, C.A., Carvanoa, J.M., Mothé-Diniz, T., Duffard, R., Florczak, M., 2004. S^3OS^2: the visible spectroscopic survey of 820] asteroids. Icarus 172, 179–220.

Levison, H., Duncan, M., 1994. The long-term dynamical behavior of short-period comets. Icarus 108, 18–36.

Love, S.G., Ahrens, T.J., 1996. Catastrophic impacts on gravity dominated asteroids. Icarus 124, 141–155.

Marzari, F., Davis, D.R., Vanzani, V., 1995. Collisional evolution of asteroid families. Icarus 113, 168–187.

Migliorini, F., Zappalà, V., Vio, R., Cellino, A., 1995. Interlopers within asteroid families. Icarus 118, 271–291.

Milani, A., Knežević, Z., 1990. Secular perturbation theory and computation of asteroid proper elements. Celest. Mech. Dyn. Astr. 49, 347–411.

Milani, A., Knežević, Z., 1992. Asteroid proper elements and secular resonances. Icarus 98, 211–232.

Milani, A., Nobili, A.-M., 1992. An example of stable chaos in the Solar System. Nature 357, 569–570.

Milani, A., Farinella, P., 1994. The age of Veritas asteroid family deduced by chaotic chronology. Nature 370, 40–42.

Milani, A., Farinella, P., 1995. An asteroid on the brink. Icarus 115, 209–212.

Milani, A., Knežević, Z., 1994. Asteroid proper elements and the dynamical structure of the asteroid main belt. Icarus 107, 219–254.

Milani, A., Nobili, A.-M., Knežević, Z., 1997. Stable chaos in the asteroid belt. Icarus 125, 13–31.

Michel, P., Benz, W., Tanga, P., Richardson, D.C., 2001. Collisions and gravitational reaccumulation: Forming asteroid families and satellites. Science 294, 1696–1700.

Michel, P., Tanga, P., Benz, W., Richardson, D.C., 2002. Formation of asteroid families by catastrophic disruption: Simulations with fragmentation and gravitational reaccumulation. Icarus 160, 10–23.

Mothé-Diniz, T., Roig, F., Carvano, J.M., 2005. Reanalysis of asteroid families structure through visible spectroscopy. Icarus 174, 54–80.

Moons, M., Morbidelli, A., Migliorini, F., 1998. Dynamical structure of the 2/1 commensurability with Jupiter and the origin of the resonant asteroids. Icarus 135, 458–468.

Morbidelli, A., 2002. *Modern Celestial Mechanics: Aspects of Solar System Dynamics*. Taylor & Francis, London.

Morbidelli, A., Nesvorný, D., 1998. Three-body mean motion resonances and the chaotic structure of the asteroid belt. Astron. J. 116, 3029–3037.

Morbidelli, A., Vokrouhlický, D., 2003. The Yarkovsky-driven origin of Near Earth Asteroids. Icarus 163, 120–134.

Morbidelli, A., Zappalà, V., Moons, M., Cellino, A., Gonczi, R., 1995. Asteroid families close to mean motion resonances: Dynamical effects and physical implications. Icarus 118, 132–154.

Morbidelli, A., Nesvorný, D., Bottke, W.F., Michel, P., Vokrouhlický, D., Tanga, P., 2003. The shallow magnitude distribution of asteroid families. Icarus 162, 328–336.

Nesvorný, D., Morbidelli, A., 1999. Numerous weak resonances drive asteroids toward terrestrial planets orbits. Icarus 139, 295–308.

Nesvorný, D., Bottke, W.F., 2004. Detection of the Yarkovsky effect for main-belt asteroids. Icarus 170, 324–342.

Nesvorný, D., Morbidelli, A., Vokrouhlický, D., Bottke, W.F., Brož, M., 2002a, The Flora family: a case of the dynamically dispersed collisional swarm?, Icarus 157, 155–172.

Nesvorný, D., Bottke, W.F., Dones, L., Levison, H.F., 2002b. The recent breakup of an asteroid in the main-belt region. Nature 417, 720–722.

Nesvorný, D., Bottke, W.F., Levison, H.F., Dones, L., 2003. Recent origin of the Solar System dust bands. Astrophys. J. 591, 486–497.

Nesvorný, D., Jedicke, R., Whiteley, R.J., Ivezić, Ž., 2005a. Evidence for asteroid space weathering from the Sloan Digital Sky Survey. Icarus 173, 132–152.

Nesvorný, D., Vokrouhlický, D., Bottke, W.F., Sykes, M.V., 2005b. Properties of asteroid dust bands and their sources. Icarus, to be submitted.

O'Brien, D.P., Greenberg, R., 2003. Steady-state size distributions for collisional populations: analytical solution with size-dependent strength. Icarus 164, 334–345.

Petit, J.-M., Farinella, P., 1993. Modelling the outcomes of high-velocity impacts between small solar system bodies. Celest. Mech. Dyn. Astr. 57, 1–28.

Pisani, E., Dell'Oro, A., Paolicchi, P., 1999. Puzzling asteroid families. Icarus 142, 78–88.

Quinn, T.R., Tremaine, S., Duncan, M., 1991. A three million year integration of the earth's orbit. Astron. J. 101, 2287–2305.

Rubincam, D.P., 2000. Radiative spin-up and spin-down of small asteroids. Icarus 148, 2–11.

Ryan, E.V., Melosh, H.J., 1998, Impact fragmentation: From the laboratory to asteroids. Icarus 133, 1–24.

Šidlichovský, M., Nesvorný, D., 1997. Frequency modified Fourier transform and its applications to asteroids. Celest. Mech. Dyn. Astron. 65, 137–148.

Stokes, G.H., Evans, J.B., Larson, S.M., 2002. Near-Earth asteroid search programs. in: *Asteroids III* (W.F. Bottke, A. Cellino. P. Paolicchi and R.P. Binzel, Eds.), pp. 45–54. Arizona University Press, Tucson.

Tanga, P., Cellino, A.;, Michel, P., Zappalà, V., Paolicchi, P., Dell'Oro, A., 1999. On the size distribution of asteroid families: The role of geometry. Icarus 141, 65–78.

Tedesco, E.F., Noah, P.V., Noah, M., Price S.D., 2002. The supplemental IRAS minor planet survey. Astron. J. 123, 1056–1085.

Tholen, D.J., 1989. Asteroid taxonomic classifcations. in: *Asteroids II* (R.P. Binzel, T. Gehrels, and M.S. Matthews, Eds.), pp. 1139-1150. Arizona University Press, Tucson.

Tsiganis, K., Varvoglis, H., Morbidelli, A., 2003. Short-lived asteroids in the 7/3 Kirkwood gap and their relationship to the Koronis and Eos families. Icarus 166, 131–140.

Tüg, H., 1977. Vertical extinction on La Silla. Messenger 11, 7–8.

Veeder, G.J., Matson, D.L., Owensby, P.D., Gradie, J.C., Bell, J.F., Tedesco, E.F., 1995. Eos, Koronis, and Maria family asteroids: Infrared (JHK) photometry. Icarus 114, 186–196.

Vokrouhlický, D., 1998. Diurnal Yarkovsky effect as a source of mobility of meter-sized asteroidal fragments. I. Linear theory. Astron. Astrophys. 335, 1093–1100.

Vokrouhlický, D., 1999. A complete linear model for the Yarkovsky thermal force on spherical asteroid fragments. Astron. Astrophys. 344, 362–366.

Vokrouhlický, D., Farinella, P., 1999. The Yarkovsky seasonal effect on asteroidal fragments: A nonlinearized theory for spherical bodies. Astron. J. 118, 3049–3060.

Vokrouhlický, D., Čapek, D., 2002. YORP–induced long–term evolution of the spin state of small asteroids and meteoroids. Rubincam's approximation. Icarus 159, 449–467.

Vokrouhlický, D., Brož, M., 2002. Interaction of the Yarkovsky-drifting orbits with weak resonances: Numerical evidence and challenges. in: *Modern Celestial Mechanics: from Theory to Applications* (A. Celletti, S. Ferraz-Mello and J. Henrard, Eds.) pp. 467–472. Kluwer Academic Publishers, Dordrecht.

Vokrouhlický, D., Nesvorný, D., Bottke, W.F., 2003. Thermal torques produce spin vector alignments among Koronis family asteroids. Nature 425, 147–151, 2003.

Vokrouhlický, D., Brož, M., Farinella, P., Knežević, Z., 2001. Yarkovsky-driven leakage of Koronis family members. I. The case of 2953 Vysheslavia. Icarus 150, 78–93.

Vokrouhlický, D., Brož, M., Morbidelli, A., Bottke, W.F., Nesvorný, D., Lazzaro, D., Rivkin, A.S., 2002, Yarkovsky footprints in the Eos family, Abstract No. 12.01 presented at the *Asteroids, Comets and Meteors* meeting, Berlin.

Vokrouhlický, D., Brož, M., Bottke, W.F., Nesvorný, D., Morbidelli, A., 2005. Yarkovsky chronology of young asteroid families. Icarus, submitted.

Xu, S., Binzel, R.P., Burbine, T.H., Bus, S.J., 1995. Small main belt asteroid spectroscopic survey: Initial results. Icarus 115, 1–35.

Zappalà, V., Farinella, P., Knežević, Z., Paolicchi, P., 1984. Collisional origin of the asteroid families: Mass and velocity distributions. Icarus 59, 261–285.

Zappalà, V., Cellino, A., Farinella, P., Knežević, Z., 1990. Asteroid families. I - Identification by hierarchical clustering and reliability assessment. Astron. J. 100, 2030–2046.

Zappalà, V., Bendjoya, P., Cellino, A., Farinella, P., Froeschlé, C., 1995. Asteroid families: Search of a 12,487-asteroid sample using two different clustering techniques. Icarus 116, 291–314.

Zappalà, V., Cellino, A., Dell'Oro, A., Migliorini, F., Paolicchi, P., 1996. Reconstructing the original velocity fields of asteroid families. Icarus 124, 156–180.

Zappalà, V., Cellino, A., Dell'Oro, A., Paolicchi, P., 2002. Physical and dynamical properties of asteroid families. in: *Asteroids III* (W.F. Bottke, A. Cellino. P. Paolicchi and R.P. Binzel, Eds.), pp. 619–631. Arizona University Press, Tucson.

Zappalà, V., Bendjoya, P., Cellino, A., Di Martino, M., Doressoundiram, A., Manara, A., Migliorini, F., 2000. Fugitives from the Eos family: First spectroscopic confirmation. Icarus 145, 4–11.

Zellner, B., Tholen, D.J., Tedesco, E.F., 1985. The eight-color asteroid survey: Results for 589 minor planets. Icarus 61, 355–416.

Table 1

Statistics of Yarkovsky-drifting orbits crossing the 7/3 MMR.

H (mag)	D (km)	N	N_c
13	9.4	102	0
14	5.9	102	6
15	3.7	102	7
16	2.4	102	13

†H and D are the absolute magnitude and size of the particles, N is the number of integrated orbits, N_c is the number of orbits that crossed the 7/3 MMR without being scattered enough in the inclination and eccentricity to remain approximately in the appropriate range of Eos members.

Table 2

Statistics of Yarkovsky-drifting orbits crossing the 9/4 MMR.

H (mag)	D (km)	N	N_c
10	37.4	102	2
11	23.6	106	6
12	14.9	102	12
13	9.4	106	15
14	5.9	106	21
15	3.7	106	30
16	2.4	106	35

†The first three columns as in Table 1 except here for the 9/4 MMR; N_c is the number of particles that were still associated with the nominal Eos family after the passage through 9/4 MMR during their further evolution.

TABLE 3

OBSERVATIONS OF THE ASTEROIDS IN THE z_1 RESONANCE ZONE (FIG. 20).

Asteroid	a (AU)	H	V_c (m/s)	ST	Date	Site
(20845) 2000 UY102	2.979	12.3	48	T	20-Jan-02	KPNO
(21211) 1994 PP36	2.976	13.41	48	T	20-Jan-02	KPNO
(33780) 1999 RU171	2.973	13.05	48	T	06-Mar-02	KPNO
(62948) 2000 VE32	2.960	13.73	58	X	22-May-03	KPNO

†Orbital data and family association (2nd through 4th columns): a is the proper semimajor axis, H absolute magnitude (AstOrb source), V_c is the critical HCM velocity cutoff at which the asteroid associates with the family.

‡ST stands for the spectral type (5th column).

⋆Observational circumstances (6th through 7th columns): UT date, observatory (KPNO stands for the 4-m Kitt Peak National Observatory telescope).

TABLE 4

OBSERVATIONS OF THE SUSPECTED INTERLOPERS IN THE EOS FAMILY (FIG. 21); DATA AS IN THE TABLE 3.

Asteroid	a (AU)	H	V_c (m/s)	ST	Date	Site
(251) Sophia	3.095	9.84	55	L	22-May-03	KPNO
(1755) Lorbach	3.092	10.74	58	T	21-Jan-02	KPNO
(2193) Jackson	3.108	10.31	60	X	23-Mar-02	La Silla
(3937) Bretagnon	3.066	11.45	55	X	22-Mar-02	La Silla
(4431) Holeungholee	3.060	11.4	65	X	20,21-Mar-02	La Silla
(8340) Mumma[a]	2.970	11.9	48	D	23-Nov-01	Palomar
(11993) 1999 XX	3.086	12.86	49	Xk	22-May-03	KPNO
(27789) 1993 BB7	3.072	12.18	45	K	08,11-Nov-02	La Silla
(36151) 1999 RG193	3.087	12.45	52	Xk	22-May-03	KPNO

[a](8340) Mumma is also the largest asteroid in the z_1 stream from the Eos family.

⋆Additional sites: Palomar (60-inch Palomar telescope), La Silla (1.52-m ESO telescope located at La Silla, Chile, operated under the agreement with the CNPq/Observatório Nacional, Rio de Janeiro).

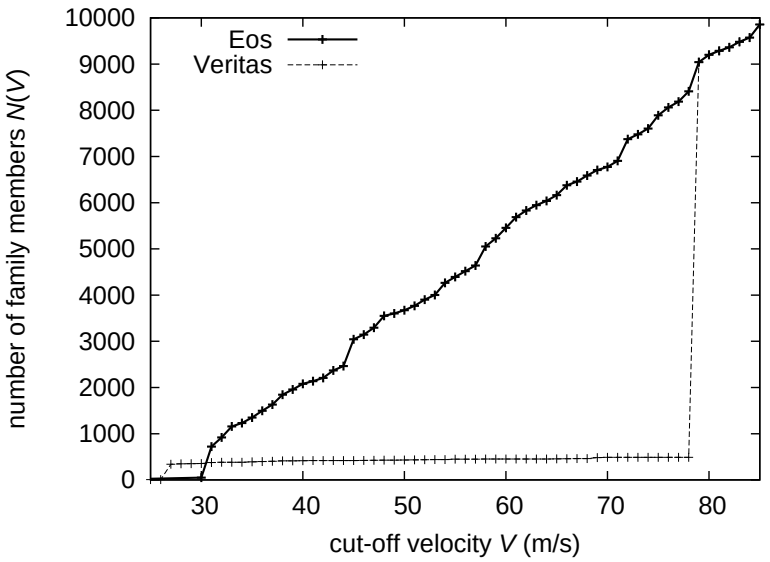

Fig. 1.— Number of asteroids associated with a family (using the HCM approach) as a function of the cut-off velocity $V_{\rm c}$ for Eos (thick line) and Veritas (thin line). The large Eos family steadily accumulates asteroids as $V_{\rm c}$ increases, while identification of the compact Veritas family shows only little dependence on $V_{\rm c}$. At a critical value of $V_{\rm c} = 78$ m/s the two neighboring families coalesce into a single structure.

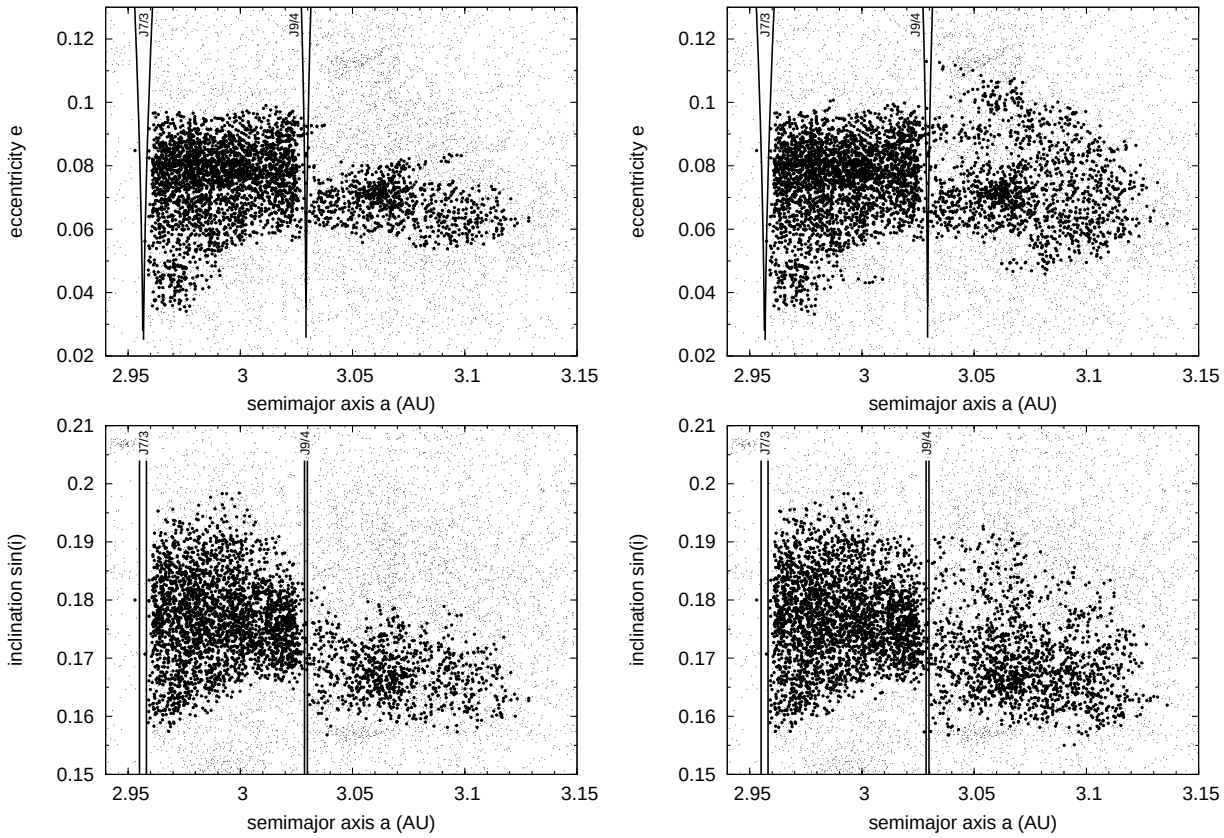

Fig. 2.— The Eos family determined by the HCM with $V_c = 50$ m/s (left figures) and 55 m/s (right figures) projected onto perpendicular planes in the space of proper elements: (i) semimajor axis a and eccentricity e (upper figures), and (ii) semimajor axis a and sine of inclination $\sin I$ (bottom figures). Family members are shown by thick symbols, while the background asteroids in a surrounding box delimited by the axes range are dots. Position of major mean motion resonances with Jupiter (7/3 and 9/4) is also shown.

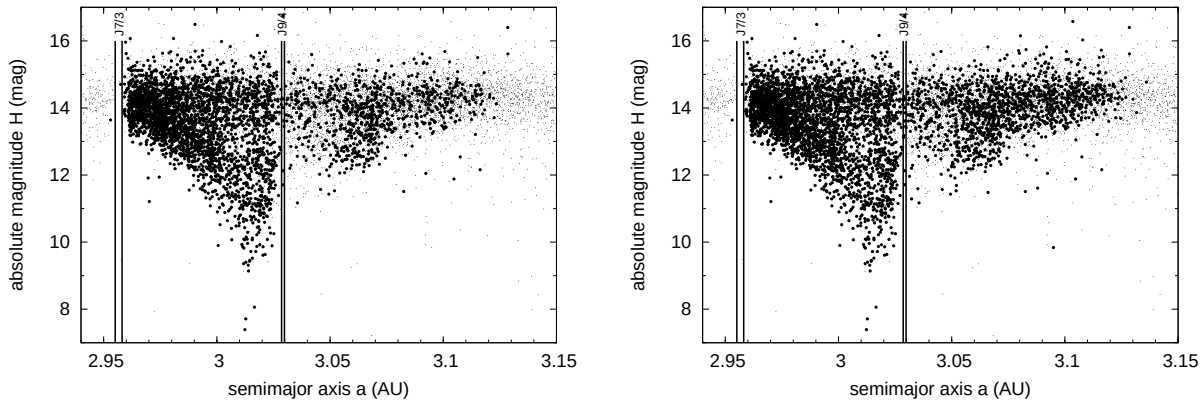

Fig. 3.— The Eos family determined by the HCM with $V_c = 50$ m/s (left) and 55 m/s (right) projected onto a plane of proper semimajor axis a and absolute magnitude H. As in Fig. 2, the family members are thick symbols, surrounding background asteroids are dots. Observation limits prevents detecting asteroids smaller than about $1 - 2$ km in size ($H \simeq 17$). Major mean motion resonances are also shown.

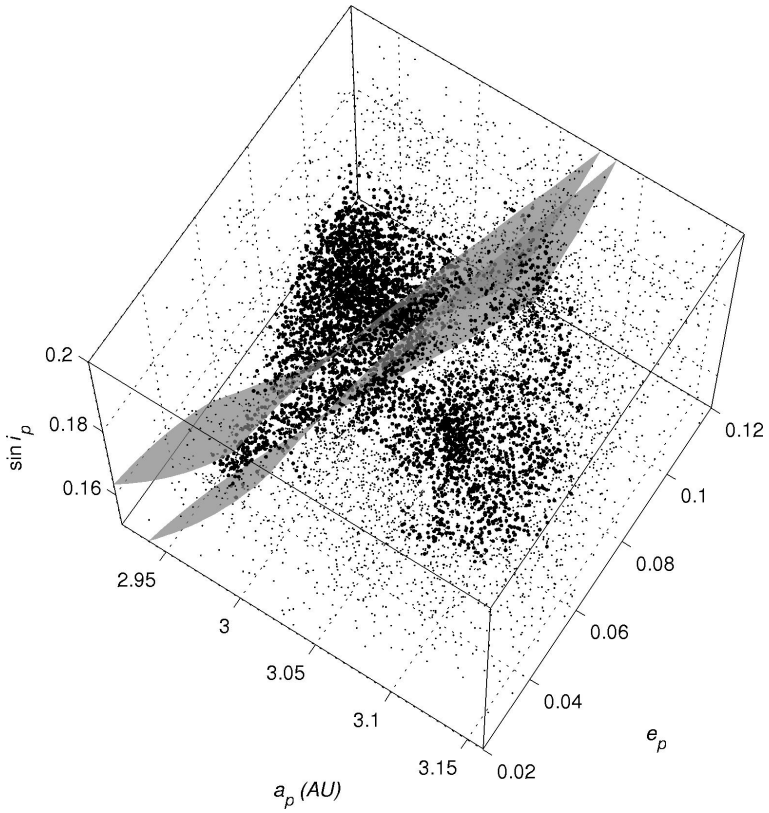

Fig. 4.— The Eos family (bold symbols) shown in 3-D space of proper orbital elements; dots are background asteroids not associated with the family by the HCM method (here $V_c = 55$ m/s is used). We emphasize existence of an asteroid stream escaping from the family toward low values of the proper eccentricity and inclination. Semi-transparent surfaces indicate approximate borders of the high-order secular resonance z_1 discussed in Sec. 3.3. We show ± 0.8 arcsec/yr region about the exact resonance whose location is determined using a semianalytic theory of Milani and Knežević (1990, 1992); this width corresponds to the numerical results from Sec. 3.3. Unlike the principal MMRs, the z_1 resonance is a strongly curved 3-D structure in the space of proper elements. The observed anomalous asteroid stream and the position of the z_1 resonance strongly correlate; this suggestive link is investigated in more detail in Sec. 3.3.

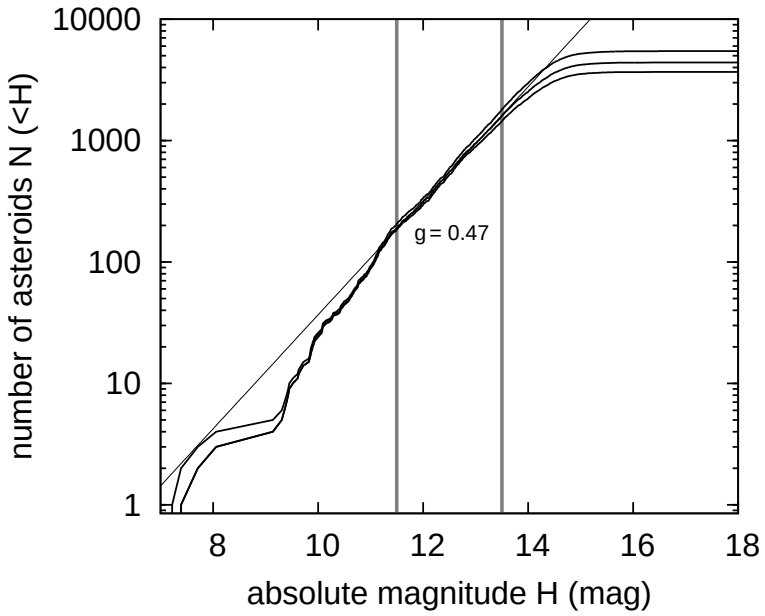

Fig. 5.— Cumulative distribution $N(< H)$ of absolute magnitude values H for members of the Eos family determined by the HCM with $V_c = 50$ m/s, 55 m/s and 60 m/s (curves from bottom to top). The straight line is a power-law approximation with index $\gamma = 0.47$ that best fits the $V_c = 55$ m/s family in the magnitude range $H \in (11.5, 13.5)$ (denoted with the two vertical lines); at larger sizes (i.e. smaller values of H) the distribution becomes steeper and dependent on individual objects, while at smaller sizes (larger values of H) the observation bias affects the data.

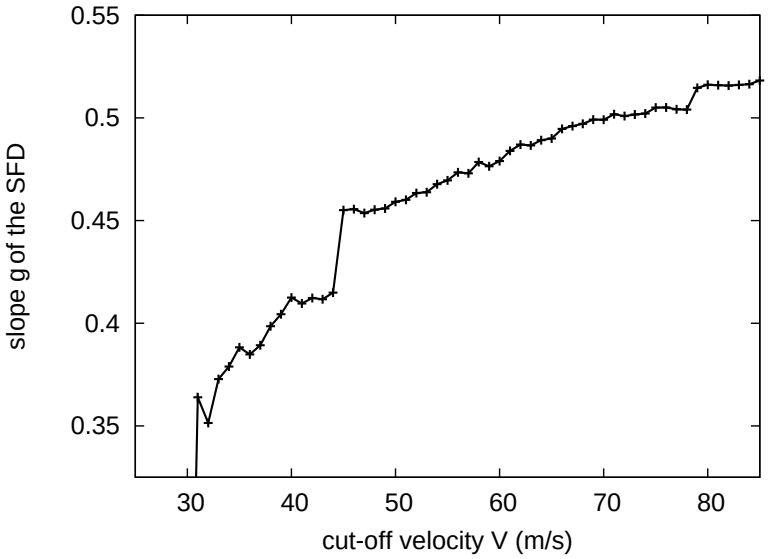

Fig. 6.— The power-law index γ of the cumulative magnitude distribution $N(< H)$ fitted in the range $H \in (11.5, 13.5)$ as a function of the HCM cut-off velocity V_c. At the largest velocity the system represents basically the whole local main-belt population around the Eos family. At any smaller value of V_c the family is shallower; at our nominal family definition of $V_c = 55$ m/s we have $\gamma = 0.47 \pm 0.02$ (see Fig. 5).

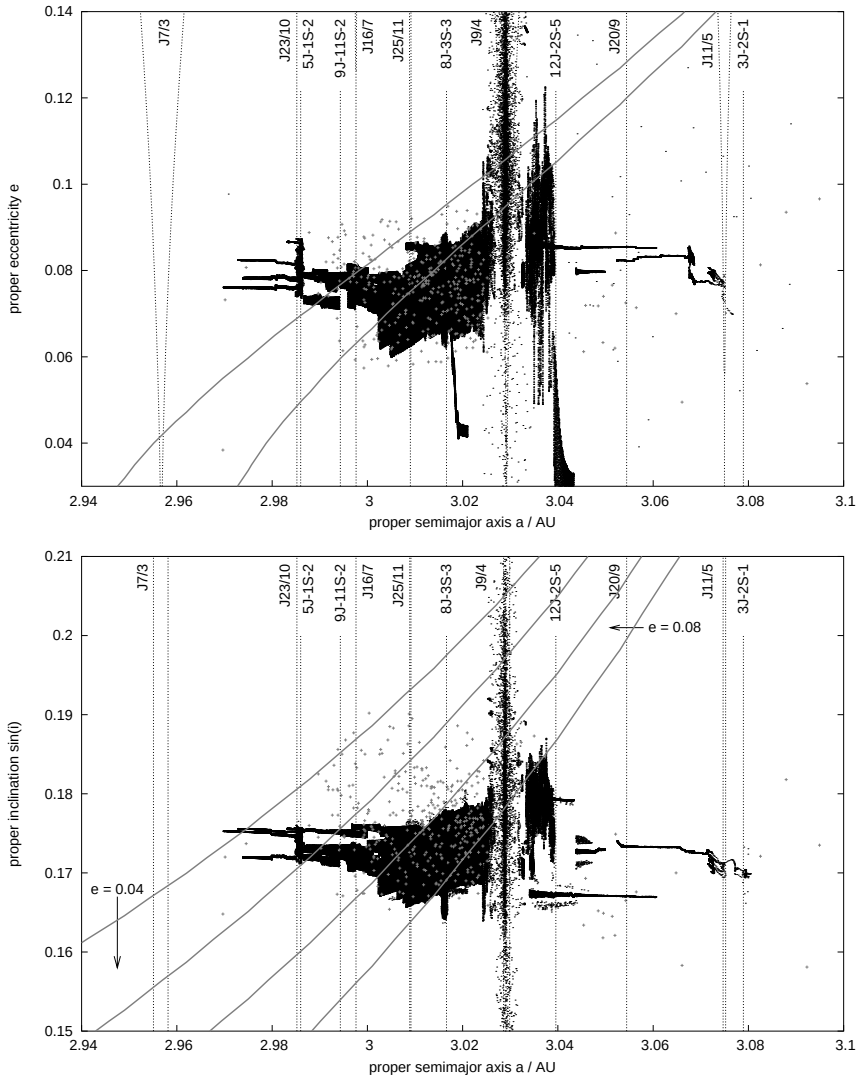

Fig. 7.— Evolution tracks of our synthetic Eos asteroids with size ≥ 7 km during 1 Gy in our simulation; dots are ≥ 7 km members of the currently observed family with the HCM threshold velocity $V_{\rm c} = 55$ m/s. Top: proper eccentricity vs. proper semimajor axis; bottom: proper sine of inclination vs. proper semimajor axis. The initially compact family extends in course of time due to a combination of the (i) Yarkovsky forces that produce diffusion in the semimajor axis, and (ii) interaction with MMRs that, upon capture, cause eccentricity and inclination to change. The latter effect is proportional to the resonance strength scaling with its order. Thus the principal resonances –here 9/4– make many of the captured asteroids eliminated from the family. Weaker MMRs, such as 16/7 or the three body resonances (shown in the figure), have not a capability to eliminate asteroids from the family, yet they can make the family to extend in eccentricity and inclination. A special effect is produced by the high-order secular z_1 resonance (Sec. 3.3) that make the Yarkovsky drifting orbits frequently captured and driven along it for a long period of time. This is because this resonance varies along all proper elements, approximately diagonally across the family. The grey curves show nominal location of the resonance ± 0.8 "/y zone for: (i) $\sin I = 0.17$ (top), and (ii) $e = 0.04$ and $e = 0.08$ (bottom).

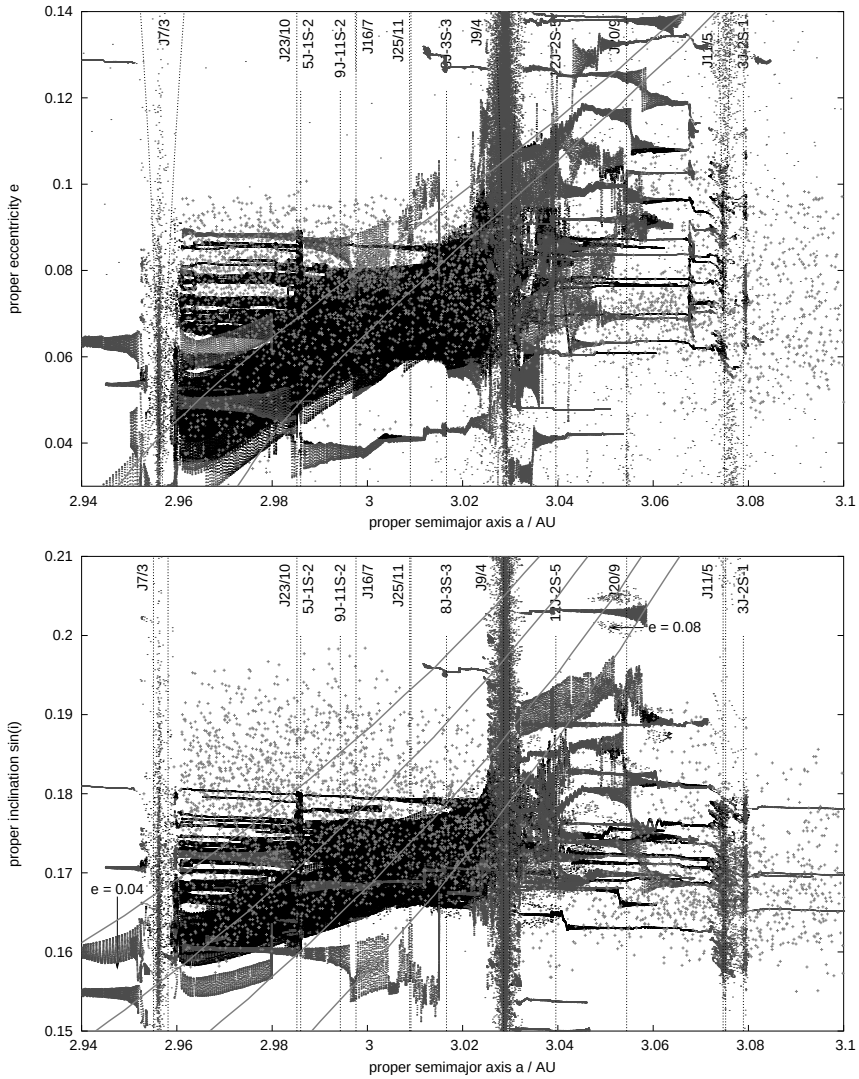

Fig. 8.— The same as in Fig. 7 but here for asteroids with size $\leq$ 7 km (view dominated by 2 km size bodies). These objects have a faster semimajor axis drift due to the Yarkovsky forces and some manage to cross the whole extend of the family in semimajor axis. As in Fig. 7 we note both interaction with the weak MMRs and significant role of the z_1 secular by trapping the migrating objects and transporting them to smaller values of proper inclination and eccentricity. With that process, nearly the complete eccentricity extend of the family is achieved, though effect on inclination is still small. Transparency of the 9/4 MMR for the migrating objects is higher now, yet many asteroids still get ejected from the Eos family via this route. The 7/3 MMR may eventually be also crossed by few of these smaller asteroids, but upon this crossing the eccentricity and inclination get largely changed. The black sections of the evolutionary tracks indicate the particle is still associated with the Eos family at the nominal HCM cut-off velocity $V_c = 55$ m/s; the dark-gray section indicate the particle escaped too far from the family and ceases to be associated with it. Note, that the few objects that crossed the J7/3 resonance became unrelated to the Eos family at the adopted nominal HCM cut-off velocity.

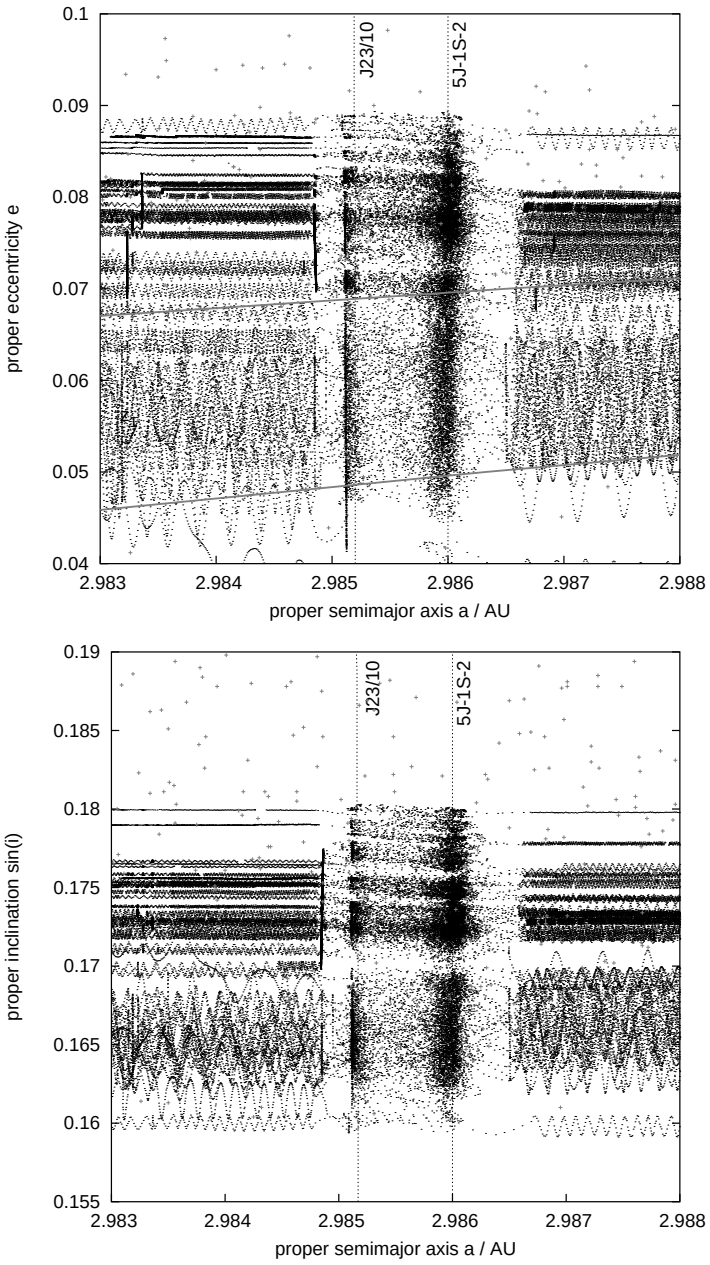

Fig. 9.— A zoom of the Fig. 7 showing tracks of particles in our simulation near a pair of weak mean motion resonances J23/10 and 5J-1S-2 (see the text for nomenclature); dots are the currently observed asteroids. Upper panel is a projection onto the proper eccentricity vs. proper semimajor axis values, lower panel gives a projection onto the proper sine of inclination vs. proper semimajor axis values. Because of the Yarkovsky forces the orbits migrate toward smaller semimajor axis values. Upon encounter the mean motion resonances, the proper eccentricity might be significantly changed; the inclination effect is quite less for these resonances. The bottommost migrating particles are trapped in the z_1 secular resonance and stay so even after a period of interaction with the mean motion resonances.

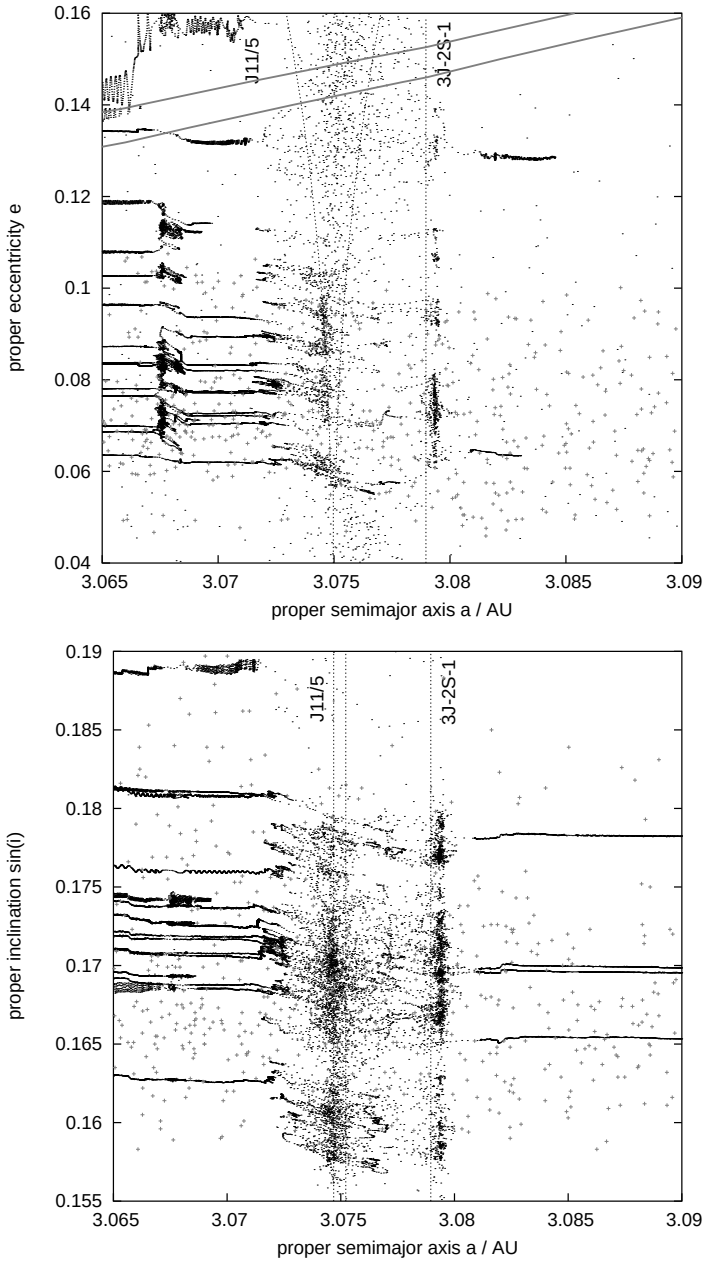

Fig. 10.— A zoom o the evolutionary paths of the Eos members in our simulation near the J11/5 and 3J-2S-1 resonances. This doublet causes a non-negligible elimination rate and only orbits at sufficiently low initial e value have a good chance to continue populating the family at $a \geq 3.08$ AU.

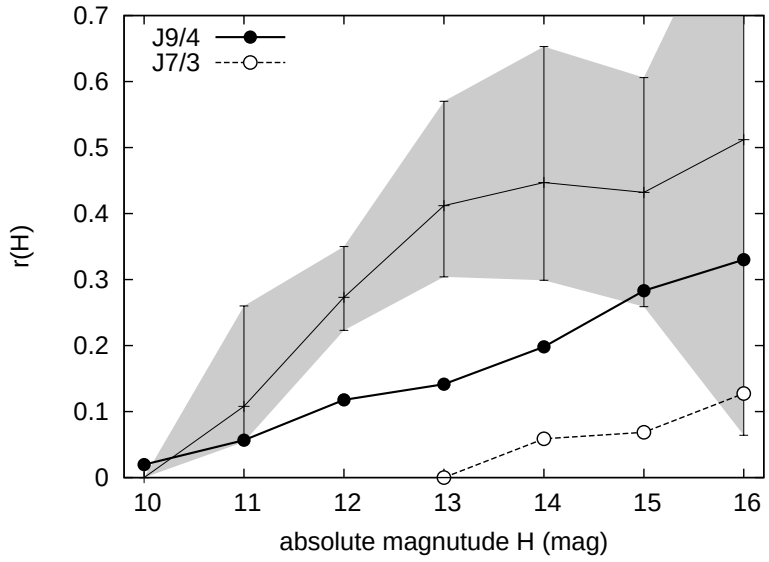

Fig. 11.— The thin line shows ratio $r(H)$, from Eq. (4), of the observed vs expected Eos members on the right over left hand sides of the 9/4 MMR as a function of the absolute magnitude H; we consider bodies binned in 0.5 zones of H about $H = 10 - 16$ with the last value, however, having large uncertainty due to few known objects only (see Fig. 3). The shaded uncertainty interval is based on computed $r(H)$ values for Eos family identifications with V_c in the range $50 - 60$ m/s (lower values for smaller V_c). Values $r < 1$ indicate a relative paucity of Eos members above the 9/4 MMR as regards to the population below the 9/4 MMR. The solid line shows probability to cross the 9/4 MMR for orbits migrating toward larger semimajor axis values by the Yarkovsky forces (symbols are data in Table 2). The lowest dashed line is the same for the 7/3 MMR.

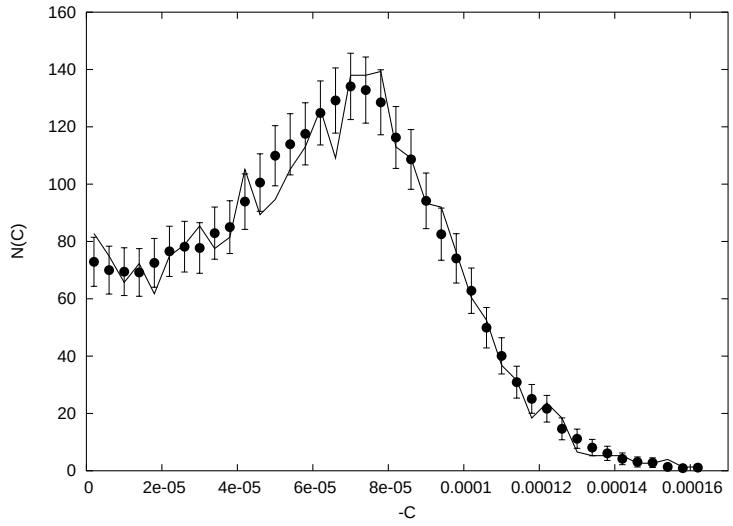

Fig. 12.— Comparison of the observed and modeled distribution $\mathcal{D}(C)$ for the Eos family; here we use model with size-independent velocity $V_{\rm SD}$ that charaterizes dispersal of the initial fragments along all directions. In fact we show directly number $N_{\rm obs}(C)$, and $N(C)$, of asteroids within a strip $(C, C + \Delta C)$ for $\Delta C = 4 \times 10^{-6}$ AU used in the target function $\Psi_{\Delta C}$ in Eq. (11). Symbols are the observed bodies $N_{\rm obs}(C)$ with the assigned formal uncertainty $\sqrt{N_{\rm obs}(C)}$; only the left branch of the family with asteroids having $a \leq a_{\rm c}$ is used here. This is an averaged result where $a_{\rm c}$ is assumed to be uniformly distributed in the range $(3.015, 3.025)$ AU. Broken solid line is our modeled family that minimizes the target function $\Psi_{\Delta C}$.

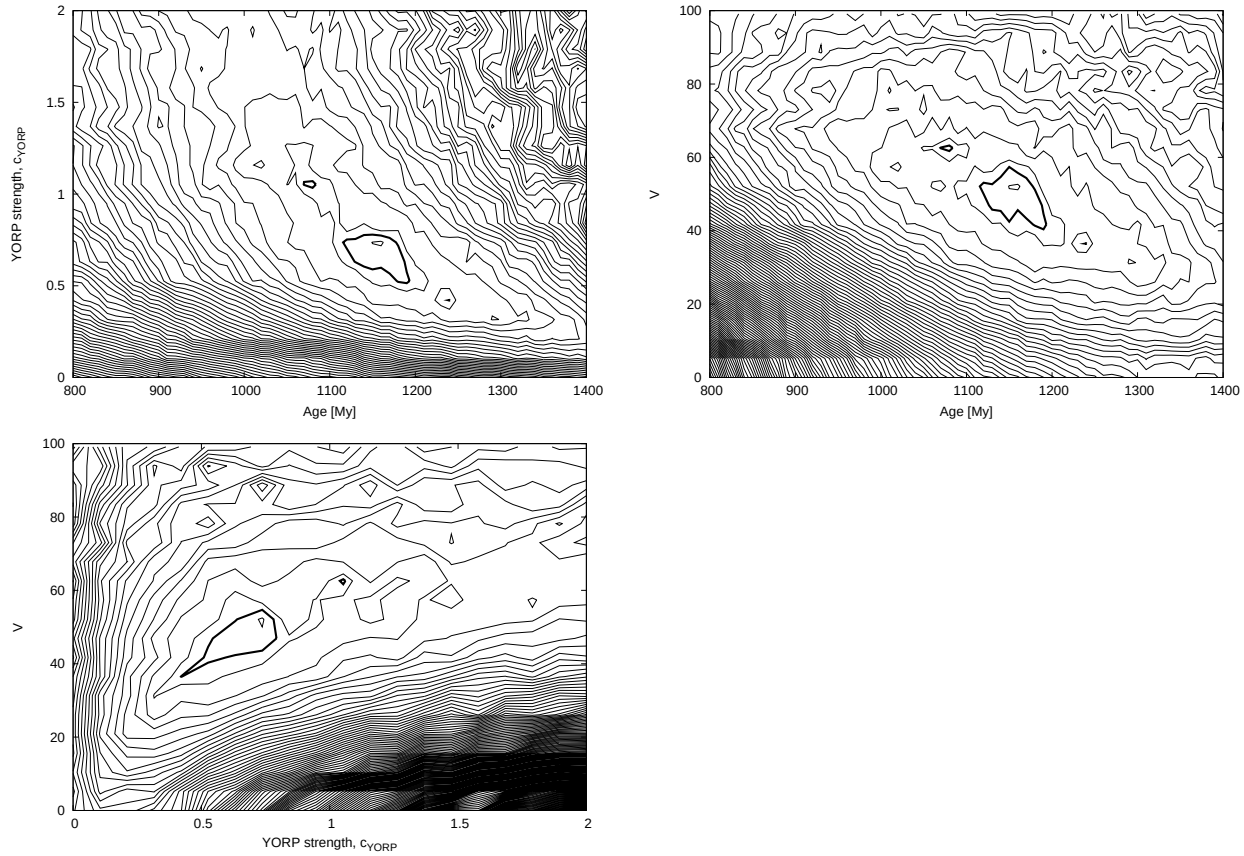

Fig. 13.— Projection of the target function $\Psi_{\Delta C}$ onto planes defined by the model parameters: (a) T vs. $c_{\rm YORP}$, (b) T vs. V, and (c) $c_{\rm YORP}$ vs. V (as in the previous figure $V_{\rm SD} = V$ is size-independent). Each time we plot the smallest $\Psi_{\Delta C}$ value along the ray of the third parameter (i.e. in the first case we fix T and $c_{\rm YORP}$ values of seek the minimum value for all tested values of V). We show several isolines of $\Psi_{\Delta C}$ with attached values (recall the best fit value is $\Psi_{\Delta C} = 27.8$, that compares to 41 bins in ΔC).

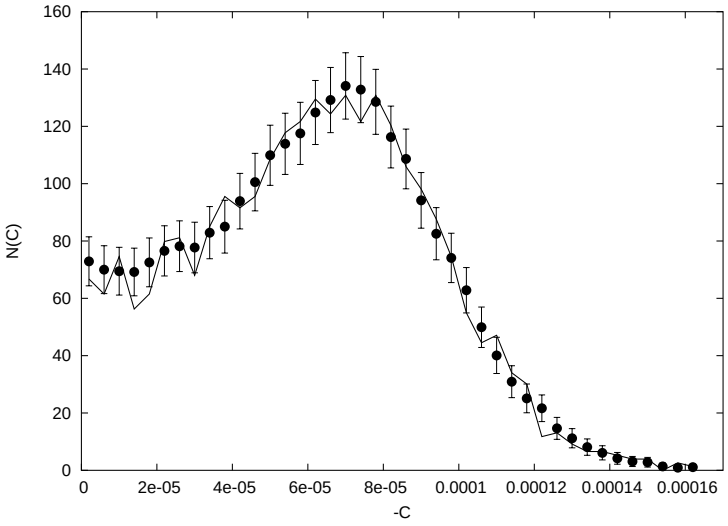

Fig. 14.— The same as in Fig. 12 but here for the model where $V_{\rm SD} = V\,(5\,{\rm km}/D)$ is size-dependent.

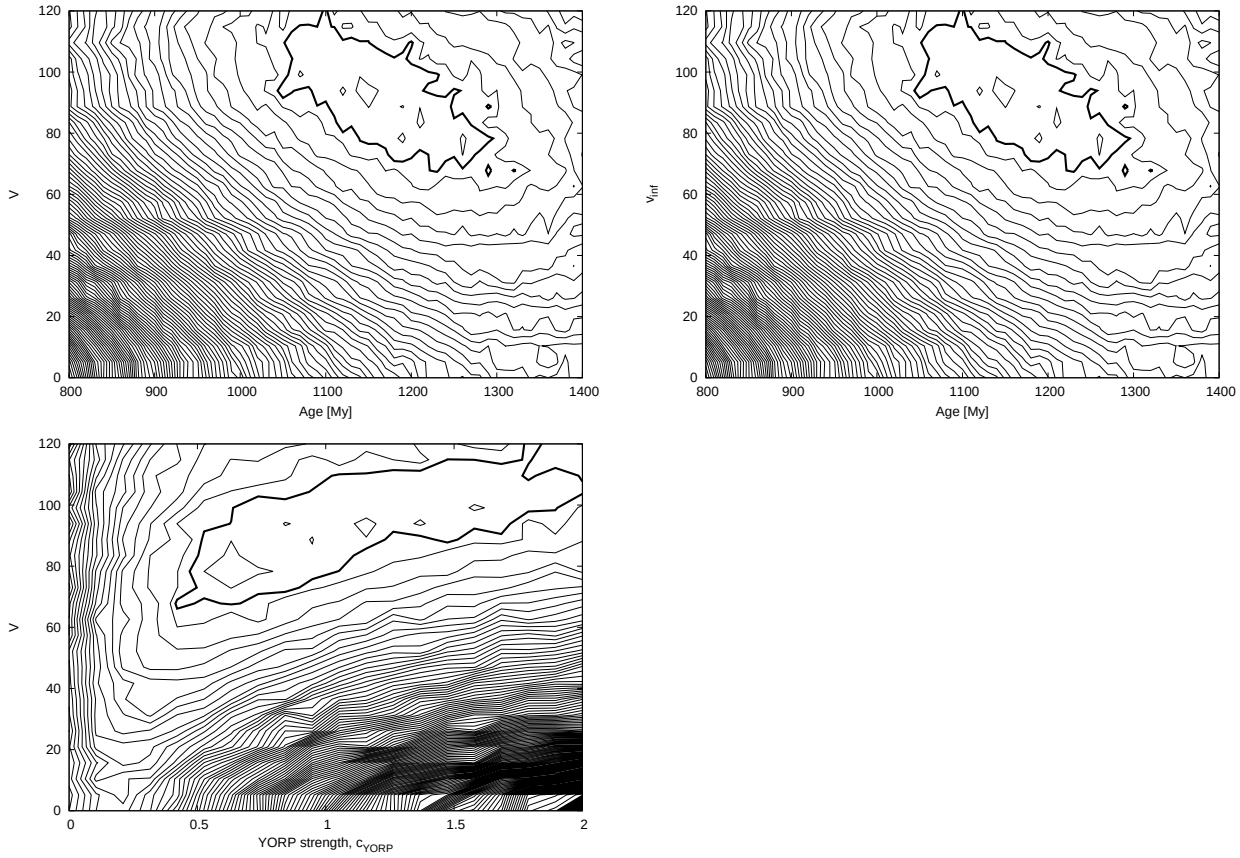

Fig. 15.— The same as in Fig. 13 but here for the model where $V_{\rm SD} = V\,(5\,{\rm km}/D)$ is size-dependent. The best-fit value is $\Psi_{\Delta C} = 26.2$.

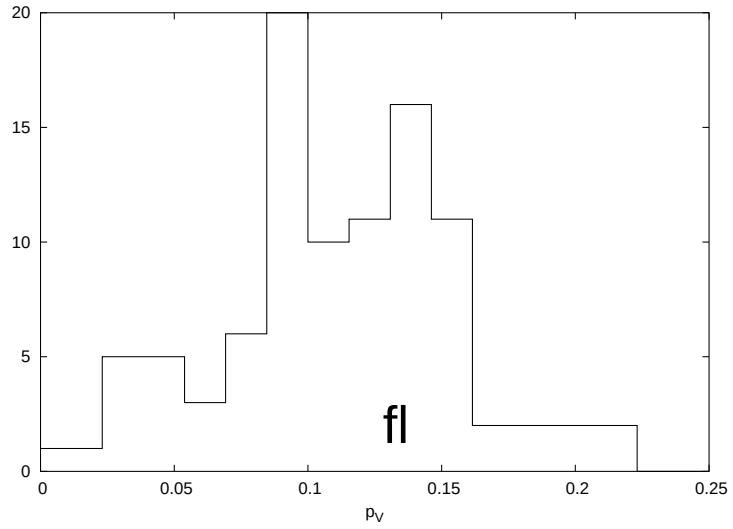

Fig. 16.— Distribution of the geometric albedo values p_V for Eos members determined by Tedesco et al. (2002); abscissa is p_V, ordinate is number of asteroids with p_V in a given bin. The arrow indicates the mean value.

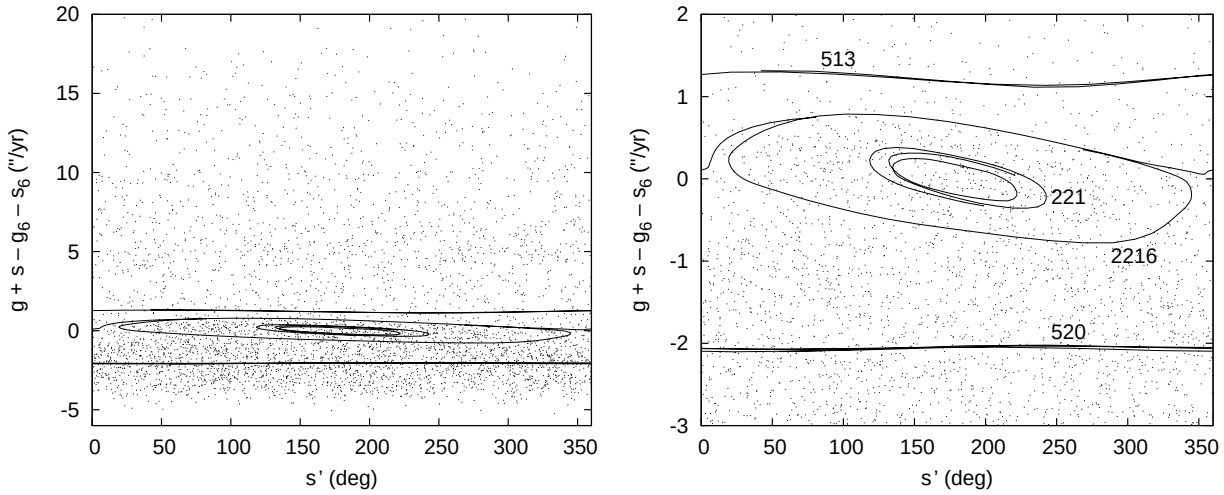

Fig. 17.— Configuration space of the z_1 secular resonance: critical angle σ' at the abscissa and secular frequency $g + s - g_6 - s_6$ on the ordinate. Left: all family asteroids included; right: zoom of the previous figure near z_1 resonance zone. Solid curves show evolution tracks of several Eos-family asteroids during our 10 My orbital integration (high-frequencies have been eliminated). The innermost librating orbit is (221) Eos itself, while other asteroids show and example of transitions between libration and circulation –(2216) Kerch– and circulations –(513) Centesima and (520) Franziska. Dots are current position of Eos asteroids (HCM family with $V_c = 55$ m/s). The negative value of $g + s - g_6 - s_6$ frequency occurs when orbital semimajor axis is smaller than the z_1 libration centre for given value of the eccentricity and inclination; thus the bulk of the family (adhering eventually to the 7/3 MMR; see Fig. 4) projects to this part of our plot.

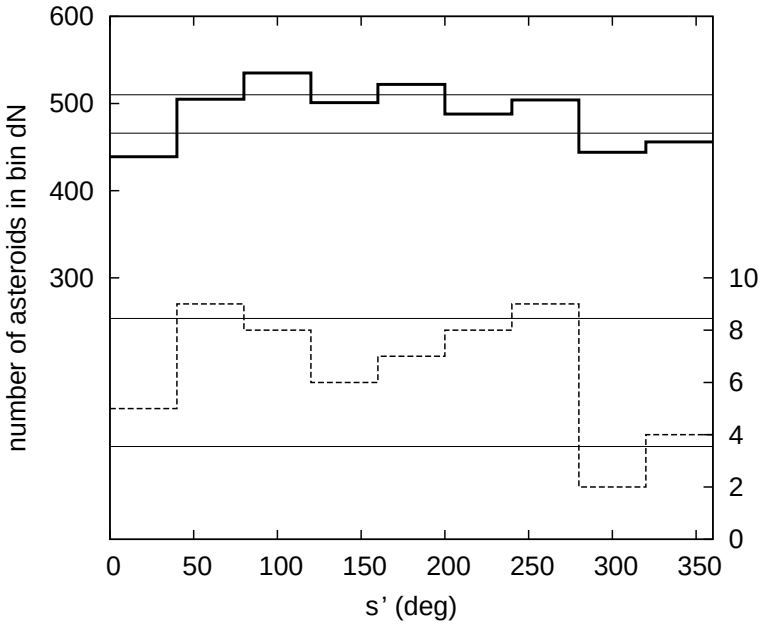

Fig. 18.— Distribution of the critical angle σ' values determined for members of our nominal Eos family (solid line and left ordinate). Previous analyses, e.g. Brouwer (1951) or Milani and Knežević (1992), found it non-uniform, suspecting a young age of the family; the dashed curve (and right ordinate) reconstructs the similar quantity for the 58 Eos members known to Brouwer (1951). Here, we show that (i) with modern data, many more asteroids added in the family, the distribution is fairly uniform, and (ii) the anomaly reported by the previous studies is due to selecting asteroids preferentially inside the z_1 resonance, for which σ' is limited to their libration interval (and the σ' values are preferentially found near extremes of the libration cycle). In each case the horizontal lines show the $\sqrt{N_m}$-uncertainty strip about the mean value N_m of the uniform distribution. If we discard asteroids residing inside the z_1 resonance, the fluctuations fit in this uncertainty strip.

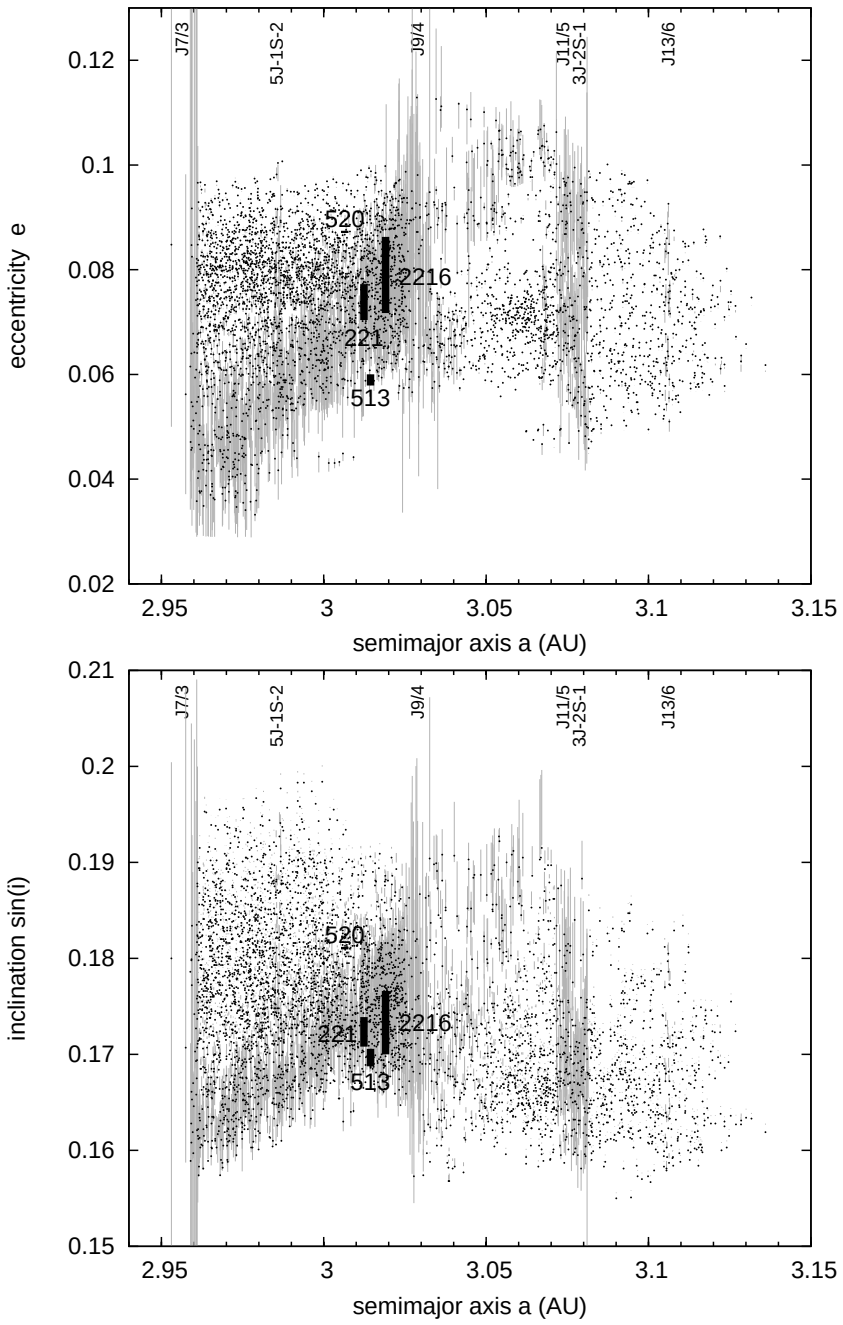

Fig. 19.— Stability of the proper elements for the nominal Eos family. In black dots we show the nominal family from proper elements of the `AstDyS` catalogue, used also in previous parts of this paper. In grey lines we show variation of the synthetic proper elements determined from our 10 My integration for all 4394 members. In particular, the grey intervals delimit minimum and maximum values of the proper elements (eccentricity e and inclination $\sin I$) determined by Fourier filtering on a running 700 ky wide window in our integration. The principal diagonal grey strip in both plots is the effect of the z_1 secular resonance. In this case, the period of e and $\sin I$ oscillation is several My (e.g. Fig. 17). Note the amplitude of the z_1 driven variation of the proper orbital elements is surprisingly large (as opposed to the resonance weakness) and it amounts to a fair fraction of the whole dispersion of the family in the appropriate elements. The thick bars are the four asteroids from Fig. 17; obviously, the largest amplitude of the oscillation occurs for (2216) Kerch, which resides near separatrix of the z_1 resonance. We also indicate effects of several MMRs, whose nomenclature is indicated at top. The most significant are effects of J7/3 and J9/4, but we can notice also J11/5 and the three-body resonance 3J-2S-1.

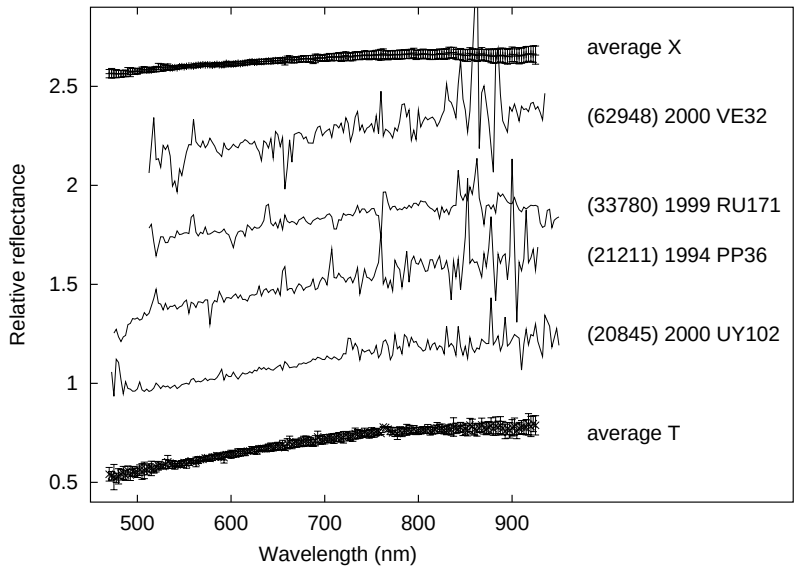

Fig. 20.— Relative reflectance spectra, normalized to unity at 550 nm, of asteroids in Table I. For (20845) UY102 the ordinate is in order, while for the other objects we arbitrarily shifted the data each time by 0.4 for visibility. For sake of comparison, we also show average reflectance spectra of T-type and X-type asteroids from the SMASS dataset (Bus and Binzel, 2002a,b, and `http://smass.mit.edu/`).

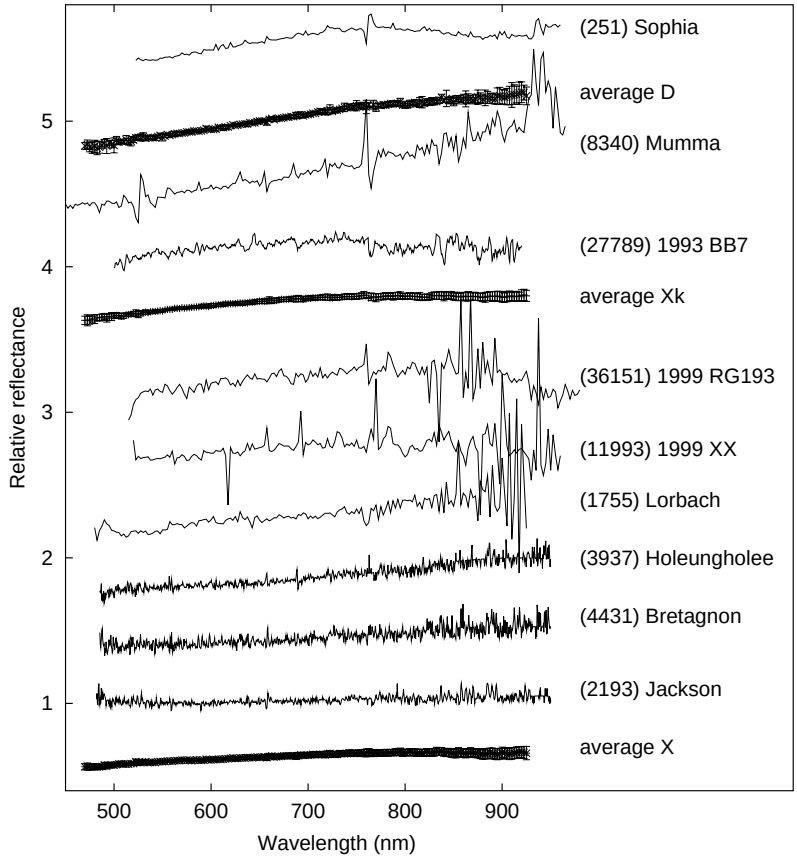

Fig. 21.— Relative reflectance spectra, normalized to unity at 550 nm, of asteroids in Table II. For (2193) Jackson the ordinate in in order, while for the other objects we arbitrarily shifted the data each time by 0.4 for visibility. Noisier data for some objects reflect their relative faintness. For sake of comparison, we also show average reflectance spectra of X-type, Xk-type and D-type asteroids from the SMASS dataset (Bus and Binzel, 2002a,b, and `http://smass.mit.edu/`).

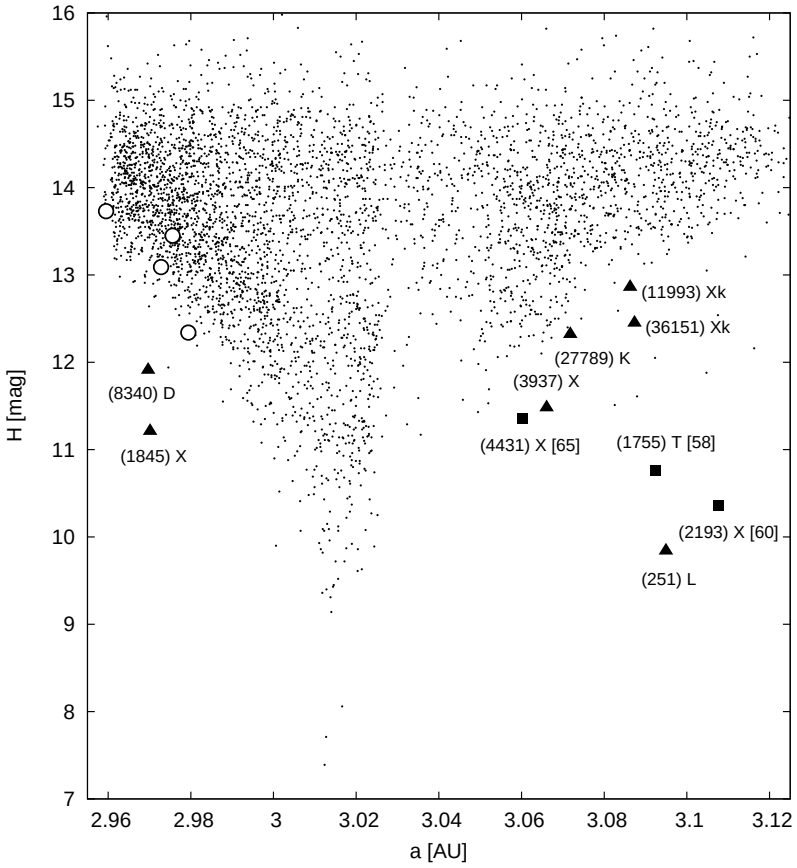

Fig. 22.— The nominal Eos family, $V_c = 55$ m/s, projected onto the plane of proper semimajor axis a and absolute magnitude H – dots. Symbols indicate position of asteroids whose spectra are reported in the paper: (i) open circles are objects inside the z_1 secular resonance (Table 1 and Fig. 20), all T-types except for (62948) 2000 VE32 which is X-type and resides nearest to the 7/3 MMR; (ii) triangles are objects nominally associated with the family but which correspond to extremal values of C parameter from Eq. (5), such that $|C| \geq 1.6 \times 10^{-4}$ AU, which are suspected interlopers; (iii) squares are the same as blue in (ii) but for asteroids associated with the Eos family at HCM cutoff velocity larger than 55 m/s. In the latter two classes we show the asteroid designation, spectral type and, in the (iii) case, the HCM cutoff velocity at which the body associates with the family (the number in squared brackets in m/s).

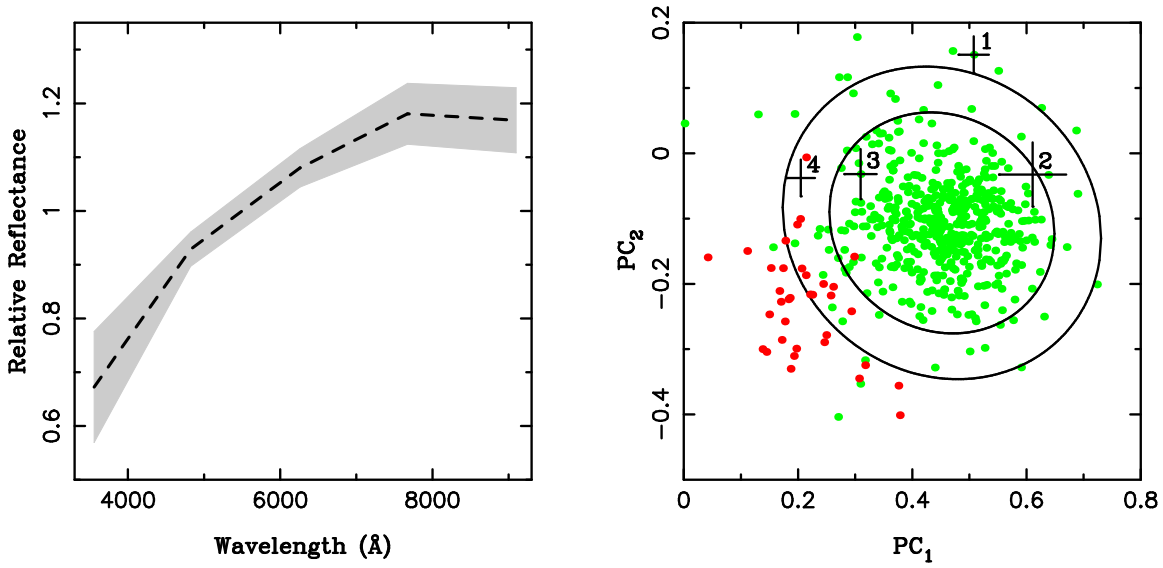

Fig. 23.— Left: Dashed curve shows a mean 5-color spectrum for 499 small Eos members from the SDSS database (release 3.0; see Jurić et al., 2002 and `http://www.astro.princeton.edu/~ivezic/sdssmoc/sdssmoc.html`) whose principal spectral components have an error smaller than 0.1 (here we normalized the result to unity at 550 nm as conventional). The shaded zone shows a standard deviation interval about the mean. Right: The Eos family members (green dots) projected onto the plane of spectral principal components PC_1 and PC_2 (e.g. Nesvorný et al., 2005a); here we use again the sample of 499 asteroids observed with SDSS with small enough errors. The two ellipses show a 90% (inner ellipse), resp. 99% (outer ellipse), confidence level of a formal relation between the two components that define the Eos family as a cluster of data in these variables. Objects outside these limits are likely alien to the family. Here we list large members in this zone: (i) 1 – (8340) Mumma, (ii) 2 – (1755) Lorbach, (iii) 3 – (4843) Megantic, and (iv) 4 – (4431) Holeungholee; the horizontal and vertical intervals show errorbars of the data. The last two were classified X-types by the narrowband spectroscopy, while (8340) Mumma received D classification and (1755) Lorbach T classification (see Fig. 21). For sake of comparison we also show the neighboring Veritas family, classified as C-type group, in red dots.